LITHOS 488–489 (2024) 107801

Contents lists available at ScienceDirect

LITHOS

journal homepage: www.elsevier.com/locate/lithos

Dating syn-orogenic exhumation of subducted continental crust: The case of the Northern Apennines

Francesco Giuntoli [a,*], Giulio Viola [a], Igor M. Villa [b,c]

[a] Dipartimento di Scienze Biologiche, Geologiche e Ambientali, Università degli Studi di Bologna, Bologna, Italy
[b] Institut für Geologie, Universität Bern, Baltzerstrasse 3, 3012 Bern, Switzerland
[c] Centro Universitario Datazioni e Archeometria, Università degli Studi di Milano Bicocca, 20126 Milano, Italy

ARTICLE INFO

Keywords:
Age dating
Microstructures
Petrochronology
Tectonic evolution
Apennines
Subduction

ABSTRACT

Dating deformation is key to unravel the evolution of orogens. Unfortunately, this is commonly challenged by the occurrence in the rock record of multiple overprinting deformation stages that lead to repeated blastesis and form multiple fabrics during both prograde and retrograde evolutions. Additionally, recrystallization is not always complete, which causes a mixture of inherited and neoblastic mineral phases. Therefore, an approach integrating age dating with microstructural and petrographic analyses is necessary to extract structurally constrained ages from the rock record. We used this approach to contribute to the long-lasting debate about exhumation of continental metamorphic units subducted to high-pressure conditions. We studied continental metasedimentary sequences of the Tuscan Metamorphic Units of the Northern Apennines (Italy) from two localities: the Island of Giglio to the west and the Monticiano-Roccastrada Unit to the east. We obtained two analytically distinct $^{40}Ar/^{39}Ar$ age ranges: an older 21–16 Ma age cluster is related to syn-orogenic top-to-the E contractional deformation occurring at ca. 1 GPa and 350 °C. A younger 15–11 Ma age group is related, instead, to exhumation to shallower structural levels and retrogression of these units to greenschist facies conditions. The interpretation of the results is based on white mica chemical compositions and rock fabrics. By integrating our results with published literature, we conclude that the investigated high-pressure continental metasedimentary sequences experienced early syn-orogenic exhumation from blueschist to greenschist facies conditions predominantly by a combination of extrusion and out- and in-sequence thrusting, with only minor contributions by extensional shearing during regional crustal thinning. Therefore, this study highlights the role of contractional fabrics in accommodating significant exhumation amounts of deeply subducted continental rocks.

1. Introduction

Orogens result from commonly long deformation histories that tend to generate complex crustal architectures by the juxtaposition of tectonic slices of very different origin. As a result, exhumed and fossil orogenic settings may contain high-pressure lithotectonic units in direct contact to non-metamorphic units, giving rise to at times hard-to-decipher tectonostratigraphic settings. The timing and modes of exhumation of high-pressure units in those settings are, therefore, generally difficult to constrain and thus remain often ill-defined, speculative and highly debated. The main mechanisms generally taken as responsible for the exhumation of deeply-seated units are: (I) extension along low-angle crustal-scale detachments (Lister and Davis, 1989), (II) return (corner) flow of low-viscosity material (Cloos, 1982) and diapirism of low-density rocks (England and Holland, 1979), (III) the response of the orogenic wedge to its possible under- or over-criticality, causing accretion by thrusting at depth and normal faulting at shallower structural levels, respectively, and their transient activation in space and time (Davis et al., 1983; Platt, 1986), (IV) out-of-sequence thrusting (Morley, 1988), (V) extrusion (Maruyama et al., 1996) and (VI) slab rollback inducing upper plate thinning (Brun and Faccenna, 2008; Dewey, 1980). Variable combinations of these mechanisms are generally taken as capable to exhume high-pressure units to very shallow structural levels, if not even to the surface, as detailed in some review articles (e.g. Kurz and Froitzheim, 2002; Platt, 1993).

Dating fabric formation in the dynamic context of orogenic wedges offers the potential to provide valuable insights that help in unravelling the tectonometamorphic evolution of orogens (e.g. Buick and Holland,

* Corresponding author.
E-mail address: francesco.giuntoli@unibo.it (F. Giuntoli).

https://doi.org/10.1016/j.lithos.2024.107801
Received 17 January 2024; Received in revised form 2 September 2024; Accepted 8 September 2024
Available online 11 September 2024

1989), although it remains challenging to link the obtained dates to specific fabric-forming events in orogenic settings, as several overprinting stages of deformation and blastesis may occur (see review of Engi et al., 2017 and references therein). Obviously, this approach necessarily requires the availability of suitable datable mineral phases in the rock record. In low-grade metasedimentary rocks, for example, $^{40}Ar/^{39}Ar$ dating on white mica has been extensively used to constrain the record of tectonometamorphic stages. This is due to the broad stability field of white mica and to its common occurrence in different rock types. Several studies used this dating technique to constrain the evolution of orogen-scale shear zones, as well as fluid ingress during retrogression of high-pressure units (Airaghi et al., 2018; Brunet et al., 2000; Montemagni et al., 2019; Rolland et al., 2009; Villa et al., 2023; Warren et al., 2012b).

In the Northern Apennines (Italy) oceanic and continental units deformed at blueschist facies conditions are juxtaposed against subgreenschist to non-metamorphic units. The Northern Apennines orogen has been mapped for over a century, such that a wealth of detailed geological studies is available. Here, we present new $^{40}Ar/^{39}Ar$ age data on white mica from structurally constrained samples from the Island of Giglio and the Monticiano-Roccastrada area, at the internal and external edge of the Tuscan Metamorphic Units, respectively, of the Northern Apennines (Fig. 1). Based on petrographic and structural considerations, we can link these new dates to deformation that took place under blueschist and subsequent retrograde greenschist facies conditions. We interpret and use the results to propose a plausible scenario for the exhumation of high-pressure units in the northern part of the Apennines.

2. Geological setting

The Northern Apennines are an active *E*-vergent fold-and-thrust belt that accommodated the convergence between the European and African

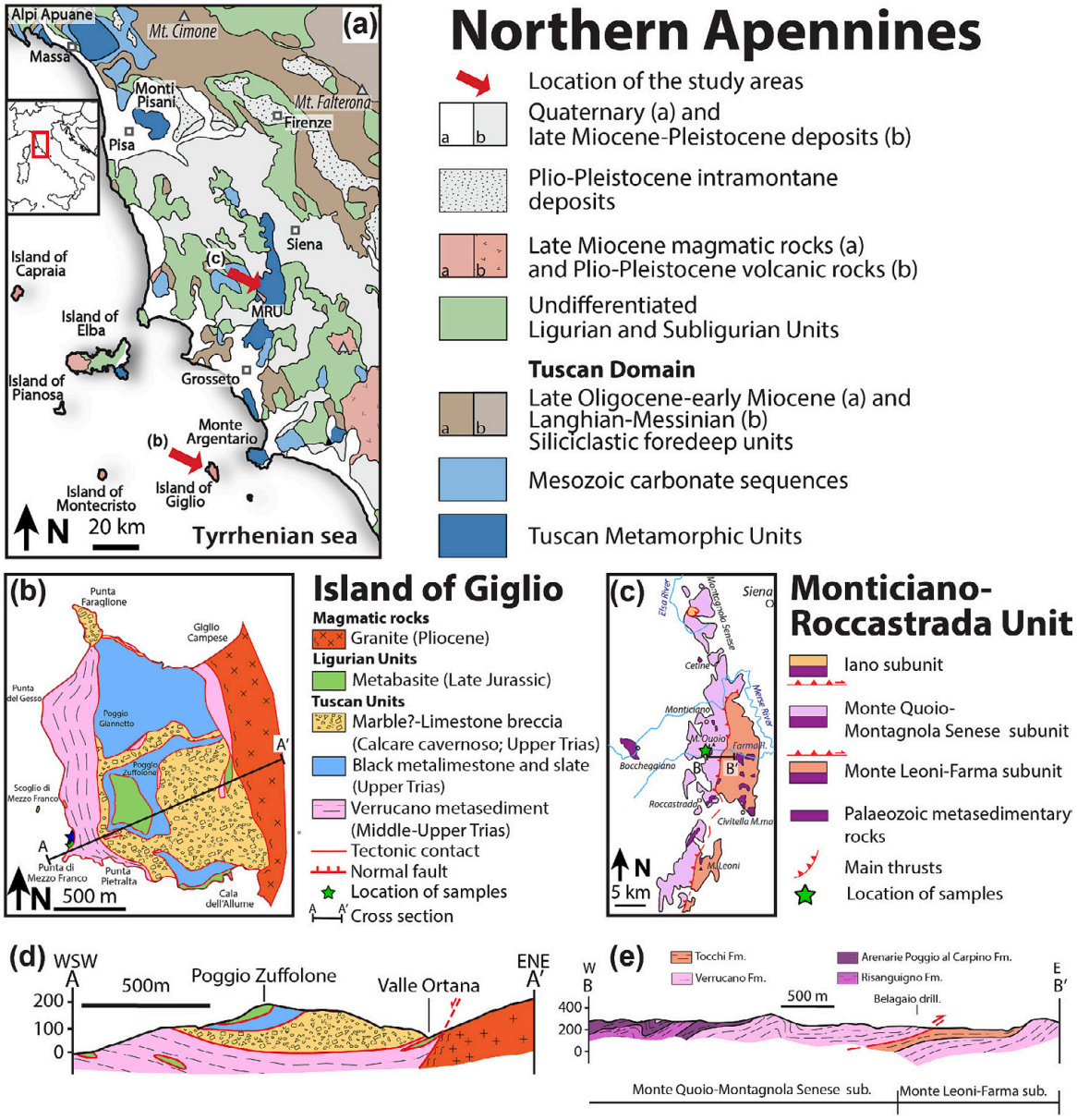

Fig. 1. (a) Simplified geological setting of the Northern Apennines (based on Conti et al., 2020). MRU: Monticiano-Roccastrada Unit. (b) Tectonic map of the Franco Promontory in the Island of Giglio (based on Lazzarotto et al., 1964; Rossetti et al., 1999. (c) Tectonic map of the Monticiano-Roccastrada Unit with the location of the study area (after Brogi and Giorgetti, 2012; Lazzarotto et al., 2003). (d) and (e) Geological cross sections of the Franco Promontory in the Island of Giglio and of the Monticiano-Roccastrada Unit, respectively (based on Lazzarotto et al., 1964; Rossetti et al., 1999 and on Casini et al., 2007). Note that only the main thrust juxtaposing the two subunits is shown in (e).

(Adria) plates from the Late Eocene Click or tap here to enter text. The Northern Apennines are formed by a nappe stack comprising, from top to bottom: i) the Ligurian Units, Ligurian Metamorphic Units and Subligurian Units, ii) the Tuscan Units and iii) the Tuscan Metamorphic Units (e.g. Carminati and Doglioni, 2012; Conti et al., 2020; Molli, 2008 and references therein; Fig. 1a). The Ligurian Units, Ligurian Metamorphic Units and Subligurian Units represent remnants of the Piedmont-Ligurian Ocean and its ocean-continent transition zone. The Ligurian Units can be further subdivided into the Internal Ligurian Units, comprising a Jurassic ophiolite sequence and a related sedimentary cover (from the Callovian to the late Cretaceous-Paleocene), and the External Ligurian Units, where ophiolites are not present; upper Cretaceous mélange units are followed upward by thick calcareous flysch and Eocene proximal turbidite-slope deposits. The Subligurian Units comprise a stratigraphic succession from the early Paleocene to early Miocene with affinity to both the External Ligurian Units and the Tuscan Nappe, reflecting their intermediate paleogeographic location. The Tuscan Units and Tuscan Metamorphic Units represent different portions of the Adria continental plate. The Tuscan Units comprise a stratigraphic succession of Triassic-early Miocene age, with marine shelf carbonate sedimentation followed, from the Sinemurian, by extension and drowning of the platform with sedimentation in pelagic conditions and, from the late Oligocene, the formation of foreland basins with deposition of turbidites. The Tuscan Metamorphic Units are composed of a metamorphosed Mesozoic-Cenozoic stratigraphic succession like the Tuscan Units with the addition of an underlying Paleozoic succession and a Paleozoic basement, the latter recording Variscan deformation.

The metamorphosed units of oceanic (Ligurian Metamorphic Units) and continental (Tuscan Metamorphic Units) origin are juxtaposed against and interleaved with non-metamorphic or sub-greenschist facies units of similar origin (Ligurian and Subligurian Units and Tuscan Nappe). These metamorphic units experienced similar conditions of 0.8–1.6 GPa and 300–500 °C between 27 and 14 Ma (Bianco et al., 2019; Di Vincenzo et al., 2022; Ryan et al., 2021 and references therein). Their exhumation and juxtaposition in the edifice of the Northern Apennines remains a matter of debate in the scientific community. A first school of thought proposes that early exhumation occurred by thrusting (Carosi et al., 2004), by thrusting at depth and normal faulting at shallower structural levels (Molli et al., 2000) and that out-of-sequence thrusting (Storti, 1995) and processes aiding extrusion in the broader subduction channel (Molli et al., 2000; Ryan et al., 2021) might have been responsible for complex tectonostratigraphic juxtapositions and significant metamorphic jumps across major tectonic contacts. On the contrary, an alternative view proposes that *syn-* and post-orogenic exhumation took place by deeply-reaching top-to-the E low-angle extensional detachments that would have acted aiding the formation of regional metamorphic core complexes and related exhumation. Continuous underthrusting of cold Adriatic units at depth would have maintained cold gradients in the subduction zone (Carmignani et al., 1994; Jolivet et al., 1998; Rossetti et al., 1999). However, some authors recently re-assessed the role of extensional exhumation and continuous exhumation since the middle Miocene. Initial extension would have occurred in the middle Miocene by low-angle normal faulting, which is responsible for significant tectonic elision in the Tuscan Nappe stratigraphic sequence and the structural superposition of the Ligurian units atop the thinned Tuscan Nappe ("Serie Ridotta"; Bertini et al., 1994). Extension would have then been followed by renewed compression in the middle to late Miocene (Bonini et al., 2014; Massa et al., 2017; Musumeci et al., 2015; Viola et al., 2018, 2022). Finally, from the late Pliocene high-angle normal faulting related to post-orogenic extension of the Northern Tyrrhenian Sea would have further exhumed the now exposed high-pressure metamorphic units by a few additional kilometres (Molli et al., 2018a).

To contribute to this topic, we dated by $^{40}Ar/^{39}Ar$ stepwise heating white micas genetically related to distinct episodes of fabric formation separated from three samples from the Island of Giglio and four samples from the Monticiano-Roccastrada Unit exposed along the Farma riverbed. The studied sample suite has been the target of complementary recent studies (Giuntoli et al., 2022; Giuntoli and Viola, 2021, 2022), and additional information is, therefore, available in those articles.

2.1. Island of Giglio

Tectonic slices of Ligurian Metamorphic Units and Tuscan Metamorphic Units crop out at the Franco Promontory on the western side of the island (Lazzarotto et al., 1964; Rossetti et al., 1999; Fig. 1b). The Tuscan Metamorphic Units are composed of a metasedimentary sequence of Middle-Lower Triassic clastic rocks assigned to the Verrucano Formation (Azzaro et al., 1976). This formation is in tectonic contact with a limestone unit of Upper Triassic age (Calcare Cavernoso Formation), metalimestone and slate (Lazzarotto et al., 1964). The Ligurian Metamorphic Units are composed of metabasite and minor marble.

The Verrucano Formation is composed of metaconglomerate and metaquartzarenite layers boudinaged within and enveloped by less competent metapelite forming a block-in-matrix fabric. Cyclic brittle and ductile deformation occurred at blueschist facies conditions at >1 GPa and 300–350 °C, forming broadly coeval mylonitic foliation and dilational shear veins (Giuntoli and Viola, 2022). A greenschist facies overprint is only locally present, and is mostly static (Giuntoli and Viola, 2022; Jolivet et al., 1998; Rossetti et al., 1999). High-angle normal faults accommodated upper crustal and post-orogenic extension and facilitated pluton emplacement (Rossetti et al., 1999). The remaining part of the island is formed by a 5 Ma old monzogranitic intrusion (Westerman et al., 1993).

2.2. Monticiano-Roccastrada Unit (MRU)

The MRU is composed of three stacked N-S trending thrust sheets that are, from structurally higher to lower and from internal to external, the Iano-, the Monte Quoio-Montagnola Senese- and the Monte Leoni-Farma subunits (Fig. 1c; Costantini et al., 1988; Lazzarotto et al., 2003). The Monte Quoio-Montagnola Senese is composed from the oldest to the youngest of the following formations: 1) the Risanguigno Formation (Lower Devonian according to Lazzarotto et al., 2003 and references therein; Middle Mississippian according to Capezzuoli et al., 2021), comprising black phyllite intercalated with dolostone beds, radiolarian chert, green metasandstone and quartzitic phyllite deposited in a marine environment; 2) the Arenarie di Poggio al Carpino Formation (Late Permian-Early Triassic) comprising quartz-rich metasandstone, metaconglomerate and minor metapelite deposited in shallow marine, inner shelf environments and shore deposits; 3) the Verrucano Formation comprising green-grey metasandstone intercalated with lenses of metaconglomerate deposited in an alluvial fan system (Lower-Middle Triassic); 4) Tocchi Formation consisting of alternating grey-greenish phyllites with yellowish-ochre to grey carbonate beds and vacuolar carbonate breccia in the upper part (Carnian; Aldinucci et al., 2008; Casini et al., 2008; Conti et al., 1991; Lazzarotto et al., 2003 and references therein).

Along the c. W-E running Farma River (Fig. 1c), a top-to-the-E/NE mesoscopic compressional duplex crops out along the riverbank (Casini et al., 2007, 2008). Coeval dilational shear veins and mylonitic foliation related to thrusting formed at blueschist facies conditions between >0.7 GPa and ca. 400 °C and ca. 1.1 GPa and 350 °C (Giuntoli and Viola, 2021). Comparable metamorphic conditions have also been reported from elsewhere in the MRU (Brogi and Giorgetti, 2012; Giorgetti et al., 1998).

3. Material and methods

3.1. Sampling strategy

Fieldwork aimed at characterizing and sampling the fabrics whose dating could shed light on the age of the recognised tectonic phases. In detail, samples were selected when the blueschist facies fabrics were clearly visible at the mesoscale and there was no trace of later overprint. In addition, for the Island of Giglio, the selected samples were collected in areas where the contact overprint of the pluton was not appreciable. Finally, every hand specimen selected to separate white mica (see below) was studied in thin section, to guarantee the sampling of the least retrogressed fabrics.

3.2. Electron probe micro-analyser (EPMA) and X-ray compositional map elaboration

Carbon-coated thin sections were analysed with a JEOL JXA-8200 electron microprobe at the Department of Earth Sciences of the University of Milano (Italy). Backscattered electron images (BSE) were acquired at an accelerating voltage of 15 keV, a beam current of 5 nA, and a working distance of 11 mm. Spot analyses and compositional maps were acquired using wavelength-dispersive spectrometers. Spot analyses were acquired at a 15 keV accelerating voltage, a 5 nA beam current and a beam diameter of ca. 1 μm. The list of the used standards contains grossular ($SiO_2/Al_2O_3/CaO$), fayalite (FeO), forsterite (MgO), K-feldspar (K_2O), omphacite (Na_2O), ilmenite (TiO_2), and rhodochrosite (MnO). Compositional maps were acquired with a 15 keV accelerating voltage, a 100 nA specimen current, and 50 ms dwell times. Si, Ti, Al, Fe, Mn, Mg, Na, Ca, and K were measured in two passes. Compositional maps were processed and produced with the XMapTools software suite (Lanari et al., 2014) and standardized using spot analyses as the internal standard to obtain concentration maps of oxide weight percentage.

3.3. White mica hand picking and $^{40}Ar/^{39}Ar$ dating

White mica grains were separated from the foliation planes and hand-picked using a metal awl. Grains were divided into a clean and inclusion-free fraction (fraction #1), although it was not possible to obtain this for all samples (see Section 4.2), and, therefore, a second fraction (#2) containing inclusion-rich white micas with abundant graphite and minor rutile (and abundant hematite in the samples of Island of Giglio) was also picked (microphotographs of the separates are available in the Supplementary). White mica grains were irradiated in the McMaster University Research Reactor (Hamilton, Canada) avoiding Cd shielding. $^{40}Ar/^{39}Ar$ stepwise heating analyses were performed using a double-vacuum resistance furnace attached to a NuInstruments Noblesse rare gas mass spectrometer at the Department of Earth and Environmental Sciences, University of Milano-Bicocca (Italy) following the analytical protocol of Villa et al. (2000) and Bosio et al. (2020). The irradiation monitor used was Fish Canyon sanidine, with an assumed age of 28.172 Ma (Rivera et al., 2011); the decay constants were those of Steiger and Jäger (1977).

Three samples from the Island of Giglio and four samples from the MRU were analysed by $^{40}Ar/^{39}Ar$ stepwise heating (see Table S1 for GPS location of samples and Table S2 for $^{40}Ar/^{39}Ar$ stepwise heating data). Note that $^{37}Ar_{Ca}$ values are available for all samples except for sample FG1921–2, as the analysis of the latter fraction was performed after the pandemic, when $^{37}Ar_{Ca}$ had already decayed. We adopted the approach of $^{40}Ar/^{39}Ar$ dating of polyphase deformation and metamorphic stages proposed by Villa et al. (2014) and later refined by Montemagni et al. (2019) and Villa et al. (2023). Common denominator three-isotope correlation diagrams were used to present and interpret age data, where each step age ($^{40}Ar^*/^{39}Ar_K$) is plotted against a chemical indicator, either Cl/K ($^{38}Ar_{Cl}/^{39}Ar_K$) or Ca/K ($^{37}Ar_{Ca}/^{39}Ar_K$). These diagrams allow to depict the mixing of two or more components (Villa and Hanchar, 2017), retrogression of phengite to muscovite and circulation of metamorphic fluid with higher Cl/K ratios (Villa et al., 2014), as well as the presence of other mineral phases, such as paragonite, characterized by higher ^{37}Ar contents than muscovite (Allaz et al., 2011). To help follow this approach (which has led to our interpretation), each figure presenting the dating results is annotated with a graphic key guiding the readers through the interpretation (e.g., Fig. 6e).

4. Results

In the following, we shortly describe the mesostructural and microstructural features of the dated samples aiming, in particular, at the characterization of microstructural sites that host the targeted white mica. This approach is propaedeutic for the interpretation of the ages that we use as constraint on the episodes of fabric formation. Complementary information can be found in Giuntoli et al. (2022) and in Giuntoli and Viola (2022 and, 2021).

4.1. Mesostructural characterization

At the Franco Promontory on the Island of Giglio (Fig. 2a), metaconglomerate, metaquartzarenite and metapelite alternate with layers ranging in thickness from a few metres to several tens of metres. The metaconglomerate and metaquartzarenite display a characteristic whitish colour and are characterized by a grain-supported primary texture. The metapelite is schistose with a shiny look on the foliation. These three rock types contain a blueschist facies mylonitic foliation, which parallels the lithological layering, leading to a composite fabric. Dilational shear veins composed of quartz and carpholite occur subparallel to the foliation (Fig. 2a). The regional foliation is pervasive and generally sub-horizontal, although it is locally folded by non- cylindrical folds with axis parallel to the regional *E*-NE/W-SW stretching lineation. Indeed, all three lithotypes contain a stretching lineation marked by isooriented quartz, carpholite and muscovite grains.

Locally, a later greenschist facies overprint occurs as mostly static. Upright, open to close folds deform the blueschist facies foliation, with axes trending E-W and discrete chlorite-decorated fractures in the hinge area. S-C/C′ structures have C and C′ planes commonly decorated by chlorite and constrain a top-to-the E sense of shear, although the opposite sense of shear also occurs (Fig. 2d).

Along the Farma River in the MRU the studied top-to-the-E/NE compressional duplex is composed of metaquartzarenite, which forms either low-strain horses or high-strain zones separating horses, and metapelite, which localizes high-strain zones (Fig. 2b). The metaquartzarenite is yellow to light grey in colour and includes lenses of metaconglomerate, a few metres thick. The metapelite is schistose with a grey to bluish colour. The blueschist facies foliation and stretching lineation, mainly defined by quartz and phyllosilicates, dips and plunges gently to the W-SW. At the mesoscale, no clear evidence of retrogression is visible.

4.2. Microstructural and microchemical characterization

On the Island of Giglio, the dated metarenite and metapelite contain a blueschist mylonitic foliation defined by quartz, muscovite and carpholite, with accessory rutile, carbonate, hematite and tourmaline, wrapping around larger detrital quartz clasts (Fig. 2c,d). Muscovite grains are turbid under plane-polarized light due to μm-sized graphite and hematite inclusions (Fig. 3 a-d). Chlorite is also found to statically grow on the blueschist facies foliation, preferentially along the carpholite and muscovite-rich bands and in aggregates a few millimetres in size. Muscovite is phengitic and has higher Si contents (denoted by square brackets and given as atoms per formula units, apfu) in the grain cores that define the blueschist facies foliation and in grains located in fold hinges ([Si] = 3.2–3.35 apfu, X_{Mg} 0.55–0.7; Group 1 Fig. 4) while lower Si content (([Si] = 3.2–3.0 apfu, X_{Mg} 0.45–0.55; Group 2) along

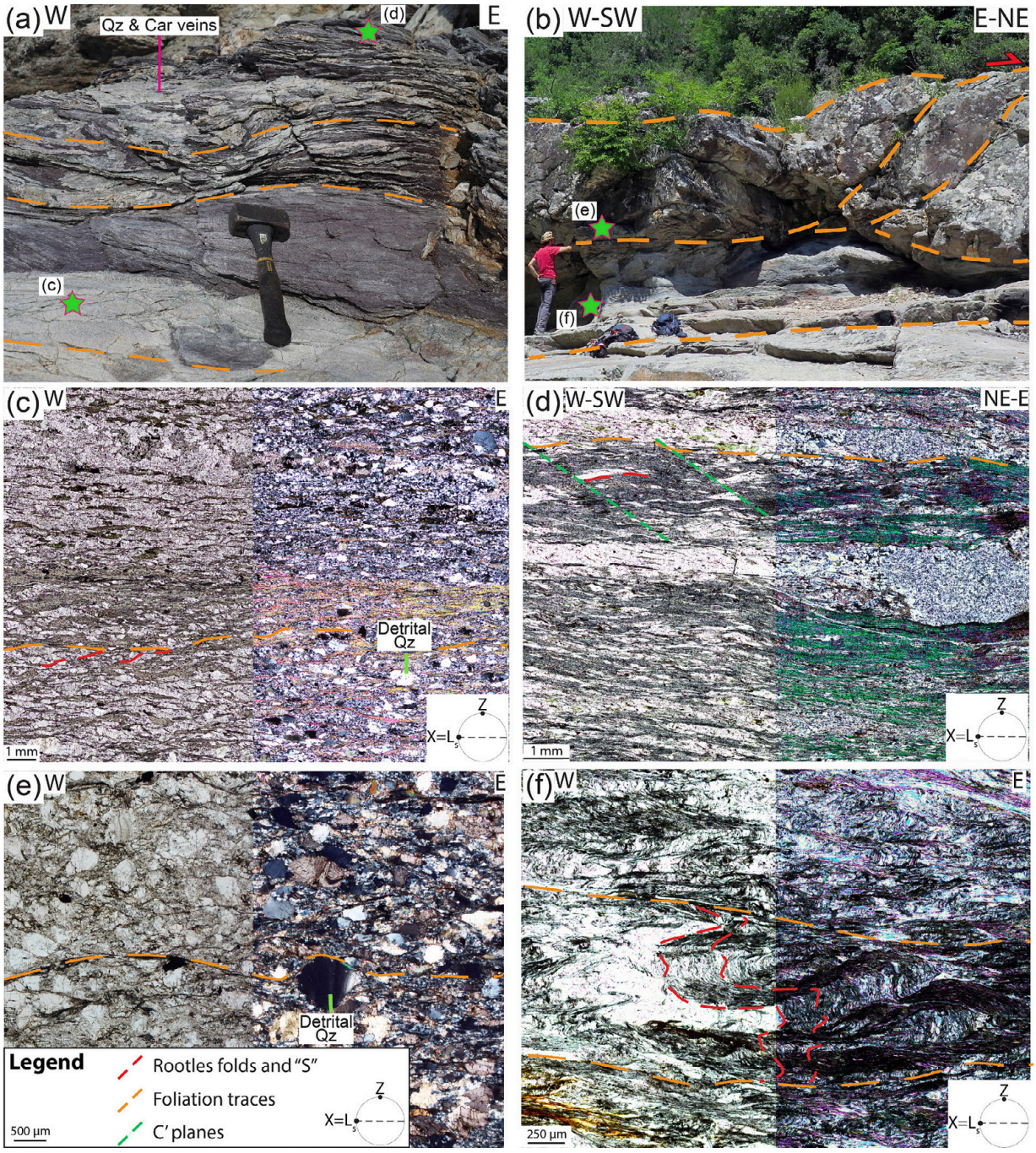

Fig. 2. Mesostructures and microstructures of the studied samples of the Island of Giglio (a,c,d) and the MRU (b,e,f), respectively. All pictures are oriented perpendicular to foliation (Z), parallel to the pole of the foliation, and parallel to the stretching lineation (X = L_s). (a) Metapelite (purple) and metarenite (white) display a blueschist facies foliation and quartz and carpholite dilational shear veins. The stars indicate the location of the studied samples. (b) Duplex outcropping along the Farma River in the MRU, with low strain metarenite horses and high strain metapelite shear zones. (c) Metarenite sample FG1941 alternates quartz-rich bands and phyllosilicate-rich bands. Larger detrital quartz grains and mica fishes display asymmetric strain shadows of a metamorphic quartz generation compatible with a top-to-the-E sense of shear. (d) Metapelite sample FG1940 shows a foliation marked by white mica, appearing turbid due to fine-grained inclusions and S-C-C′ structures compatible with a top-to-the-E sense of shear. Note the chlorite growing statically on the earlier fabric. (e) Metarenite sample FG1921 is characterized by a blueschist facies foliation marked by white mica and chloritoid wrapping around angulous detrital quartz clasts. (f) Metapelite sample FG1923 shows fold hinges, commonly rootless, and a crenulation cleavage. Both structures are marked by white mica, appearing turbid due to fine-grained inclusions, and chloritoid. (For interpretation of the references to colour in this figure legend, the reader is referred to the web version of this article.)

grain boundaries associated with chlorite, attests to retrograde greenschist facies conditions. Chemical analyses of phengitic muscovite for selected areas of these two groups extracted from compositional maps (see Fig. 4a for location) and representative spot analyses are reported in Table 1.

In the MRU, the dated metarenite and metapelite contain a blueschist mylonitic foliation marked by isooriented white mica, quartz, pyrophyllite, chloritoid, rutile and carbonate, with carpholite found only in the metarenite (Figs. 2c,d and 3 e-h). White mica grains generally appear turbid under plane-polarized light due to µm-sized graphite, rutile and pyrite inclusions. Microlithons of white mica and chloritoid grains are oriented generally at high angle to the main foliation and are wrapped

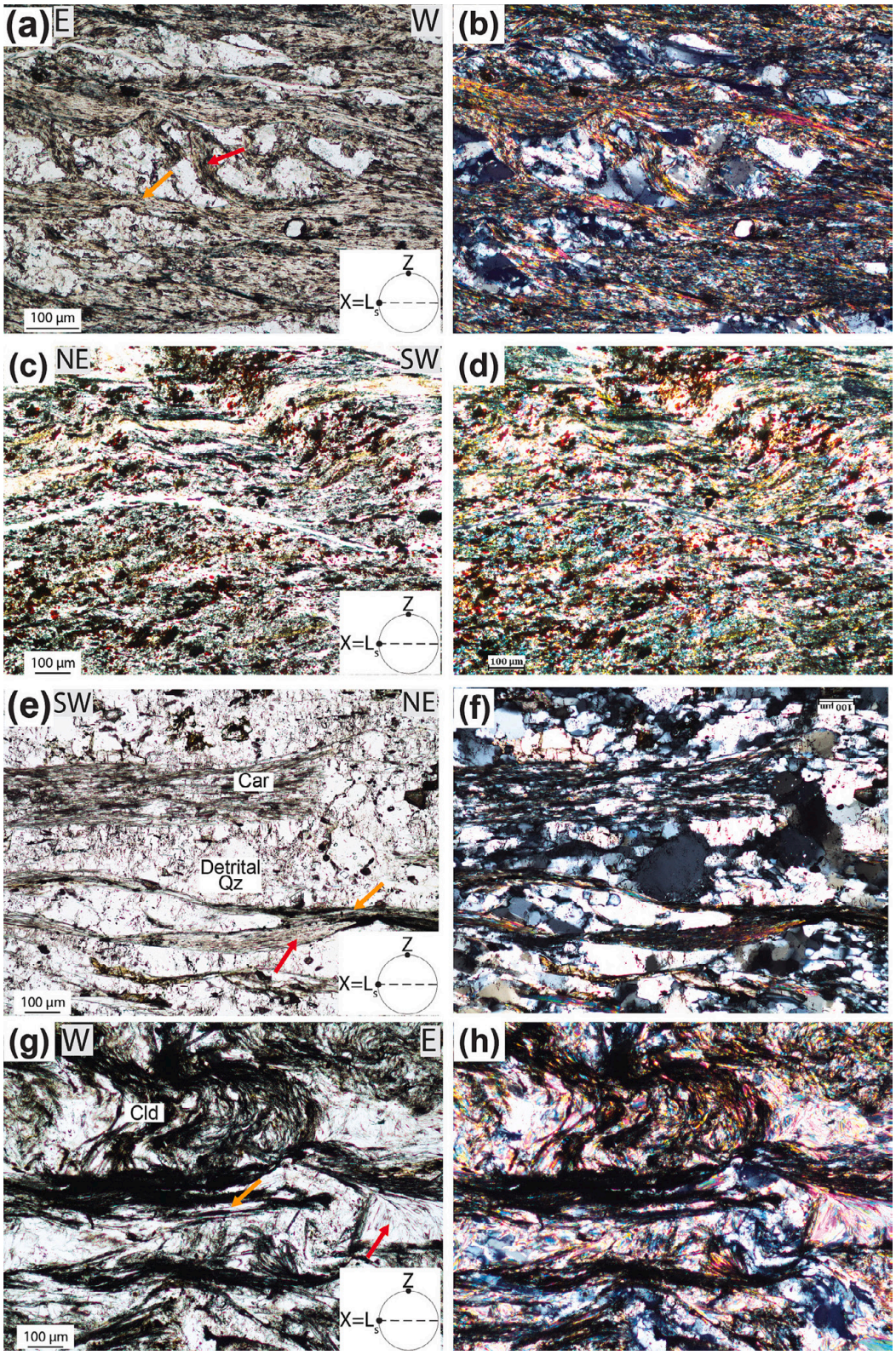

Fig. 3. Detail of white mica generations in the studied samples of the Island of Giglio (a-d) and the MRU (e-h), respectively. (a,b) Metarenite sample FG1941 displays two generations of white mica: mica fish (red arrow) and a generation parallel to the main foliation (orange arrow). (c,d) Metapelite sample FG1938 displays white mica appearing turbid due to hematite and graphite inclusions. (e,f) Metarenite sample FG1924 shows a foliation marked by white mica (orange arrow) and carpholite wrapping around detrital quartz and larger mica fish (red arrows). (g,h) Metapelite sample FG1923 displays fold hinges with larger white mica (red arrow) and chloritoid and an axial plane foliation marked by smaller white mica grains (orange arrow). (For interpretation of the references to colour in this figure legend, the reader is referred to the web version of this article.)

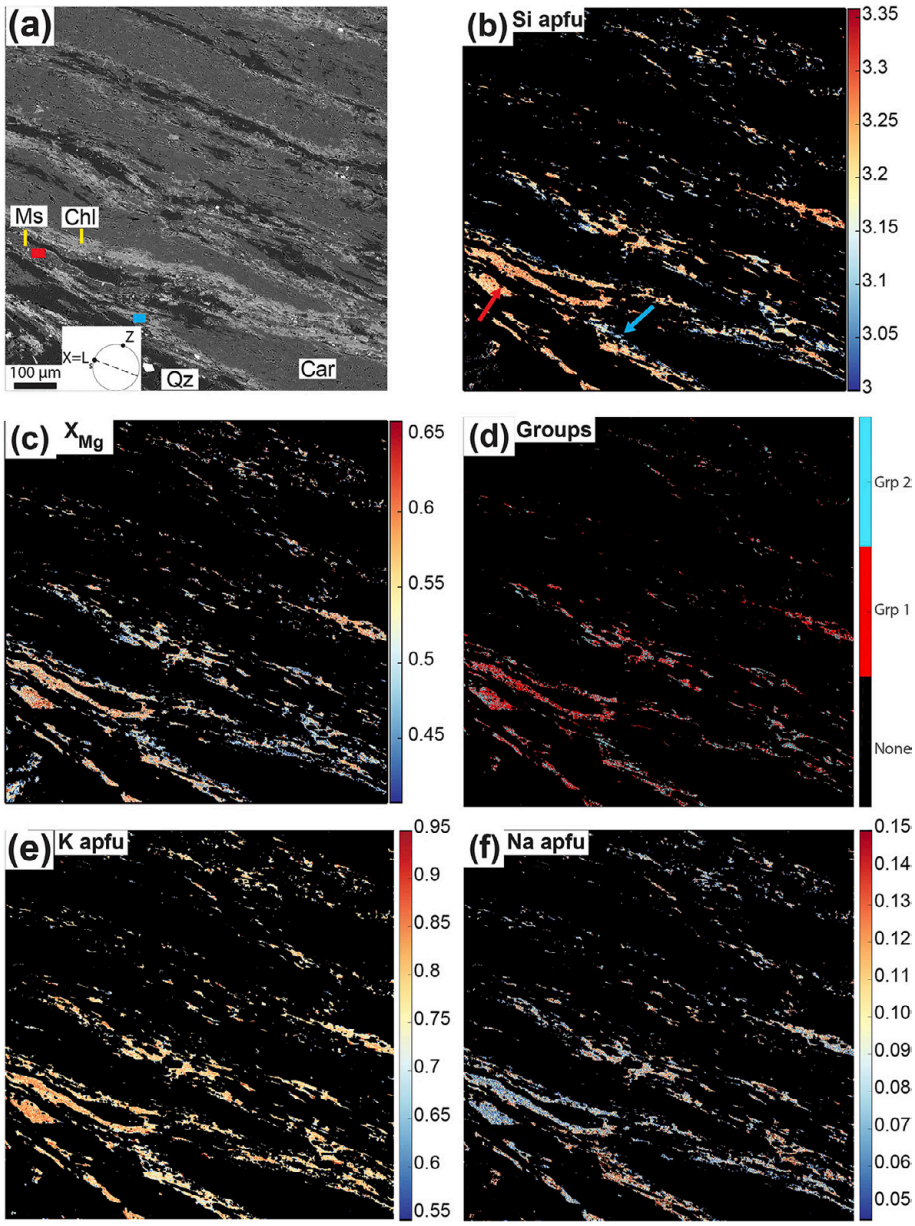

Fig. 4. (a) Backscattered electron image of metapelite sample FG1942 from the Island of Giglio. Note chlorite replacing carpholite at grain boundaries. Compare with Fig. 7 of Giuntoli and Viola (2022). Red and light blue rectangles refer to high and low Si apfu muscovite areas presented in Table 1. (b-f) X-ray compositional map of muscovite. (b) Si apfu, high and low Si contents (located in proximity of chlorite) shown by the red and light blue arrows, respectively. (c) X_{Mg} content. (d) Distinction in two groups based on the Si content (see text). (e) K apfu. (f) Na apfu. (For interpretation of the references to colour in this figure legend, the reader is referred to the web version of this article.)

by it (Fig. 3 e-h). Detrital monocrystalline or polycrystalline quartz clasts are present and are more abundant in the coarser metasedimentary layers. S-C/C′ structures and asymmetric folds indicate top-to-the E kinematics (Fig. 2f). Phengitic muscovite grains display complex chemical variations, with cores or areas higher in [Si] content (3.2–3.3 apfu; X_{Mg} 0.55–0.8; Group 1 Fig. 5) and lower [Si] content along grain boundaries (3.0–3.2 apfu; X_{Mg} 0.45–0.55; Group 2), likely marking retrogression to greenschist facies conditions (Table 1 and Fig. 5a for location). We note that the spread of the points in the selected areas in the exemplary samples chosen from Giglio and Farma is actually intrinsically complex. To find the median of each of the four analysed areas, we ordered the spot analyses by the Si concentration, as Si substitution is the reliable indicator of HP micas. However, if we choose the Mg or Fe concentrations (monitors of retrogression), the maximum Mg and Fe concentrations for the HP population are obtained in different spots from the spots having the minimum Si concentrations. Specularly, minimum concentrations of Mg and Fe in the retrograde muscovite population are obtained in other spots than those with the highest Si. We interpret this as a result of sub-µm intergrowths of HP and retrograde micas. The observation that our samples contain a neoblastic mica and a significantly resolved retrograde mica is quantified by our EPMA analyses. For each element map we acquired about 70,000 and 200,000 points and plotted them in histograms (Supplementary Fig. 1) and in a bivariate plot of the sum ($Al_{tot} + Mg + Fe$) versus Si (Supplementary Fig. 1a,b and e,f). What the data unambiguously show is that the histograms of the major element concentrations follow unsymmetric, skewed distributions with concave and convex slopes (Supplementary Fig. 1c,d and g,h). Moreover, the spread of the Si and Al concentrations is well over 6 %, whereas the nominal analytical reproducibility of the EPMA analyses of Si and Al is about 1 %. Both observations are clearly not consistent with a

Table 1
Muscovite chemical composition analyses of the selected areas (100, 80, 38 and 50 points, respectively; note that minimum, maximum and median are referred to the SiO_2 content) and representative spot analyses (wt%). See location of the selected areas in Figs. 4a and 5a.

	MUSCOVITE															
Sample	Island of Giglio								MRU							
Wt%	Group 1: High [Si]				Group 2: Low [Si]				Group 1: High [Si]				Group 2: Low [Si]			
	Spot analysis	Min	Max	Median	Spot analysis	Min	Max	Median	Spot analysis	Min	Max	Median	Spot analysis	Min	Max	Median
SiO_2	49.53	47.25	50.48	49.23	47.12	44.09	49.03	46.86	47.99	47.30	49.90	48.83	46.11	43.98	47.20	45.51
TiO_2	0.24	0.02	0.12	0.14	0.18	0.07	0.19	0.17	0.11	0.32	0.28	0.32	0.32	0.09	0.17	0.09
Al_2O_3	32.87	33.15	31.05	32.43	32.04	32.30	33.17	33.28	37.04	36.64	33.94	34.98	37.35	36.58	36.02	36.31
FeO	1.91	1.72	1.68	2.33	2.41	5.16	1.87	3.06	0.53	0.33	0.75	0.27	0.92	0.93	0.93	0.66
MnO	0.04	0.04	0.04	0.05	0.00	0.07	0.06	0.03	0.02	0.01	0.02	0.04	0.00	0.06	0.04	0.07
MgO	1.36	1.31	1.50	1.47	1.68	2.37	0.93	1.47	0.49	0.89	0.82	1.09	0.50	0.68	0.41	0.51
CaO	0.19	0.37	0.12	0.14	0.16	0.11	0.12	0.09	0.08	0.06	0.06	0.04	0.02	0.06	0.04	0.05
Na_2O	0.62	0.46	0.29	0.69	0.32	0.64	1.56	0.98	0.83	1.40	0.91	1.45	1.00	0.32	1.34	0.22
K_2O	9.47	9.63	10.08	9.63	9.87	9.24	8.95	9.07	9.03	8.98	9.90	8.29	9.63	11.66	9.75	11.19
Total	96.24	93.95	95.36	96.11	93.79	94.05	95.88	95.01	96.12	95.93	96.58	95.31	95.85	94.36	95.90	94.61
Formulae based on 11 Oxygens																
Si	3.24	3.18	3.33	3.24	3.19	3.03	3.22	3.14	3.11	3.09	3.24	3.19	3.03	2.98	3.10	3.05
Ti	0.01	0.00	0.01	0.01	0.01	0.00	0.01	0.01	0.01	0.02	0.01	0.02	0.02	0.00	0.01	0.00
Al	2.54	2.63	2.42	2.52	2.56	2.62	2.57	2.62	2.83	2.82	2.60	2.69	2.89	2.92	2.79	2.87
Fe^{2+}	0.10	0.10	0.09	0.13	0.14	0.30	0.10	0.17	0.03	0.02	0.04	0.01	0.05	0.05	0.05	0.04
Fe^{3+}	0.00	0.00	0.00	0.00	0.00	0.00	0.00	0.00	0.00	0.00	0.00	0.00	0.00	0.00	0.00	0.00
Mn	0.00	0.00	0.00	0.00	0.00	0.00	0.00	0.00	0.00	0.00	0.00	0.00	0.00	0.00	0.00	0.00
Mg	0.13	0.13	0.15	0.14	0.17	0.24	0.09	0.15	0.05	0.09	0.08	0.11	0.05	0.07	0.04	0.05
Ca	0.01	0.03	0.01	0.01	0.01	0.01	0.01	0.01	0.01	0.00	0.00	0.00	0.00	0.00	0.00	0.00
Na	0.08	0.06	0.04	0.09	0.04	0.09	0.20	0.13	0.10	0.18	0.11	0.18	0.13	0.04	0.17	0.03
K	0.79	0.83	0.85	0.81	0.85	0.81	0.75	0.77	0.75	0.75	0.82	0.69	0.81	1.01	0.82	0.96
$\sum$ cations	6.91	6.95	6.89	6.94	6.97	7.10	6.96	6.99	6.89	6.95	6.91	6.89	6.98	7.09	6.99	7.01
X_{Mg}	0.56	0.58	0.61	0.53	0.55	0.45	0.47	0.46	0.63	0.83	0.66	0.88	0.49	0.55	0.43	0.55

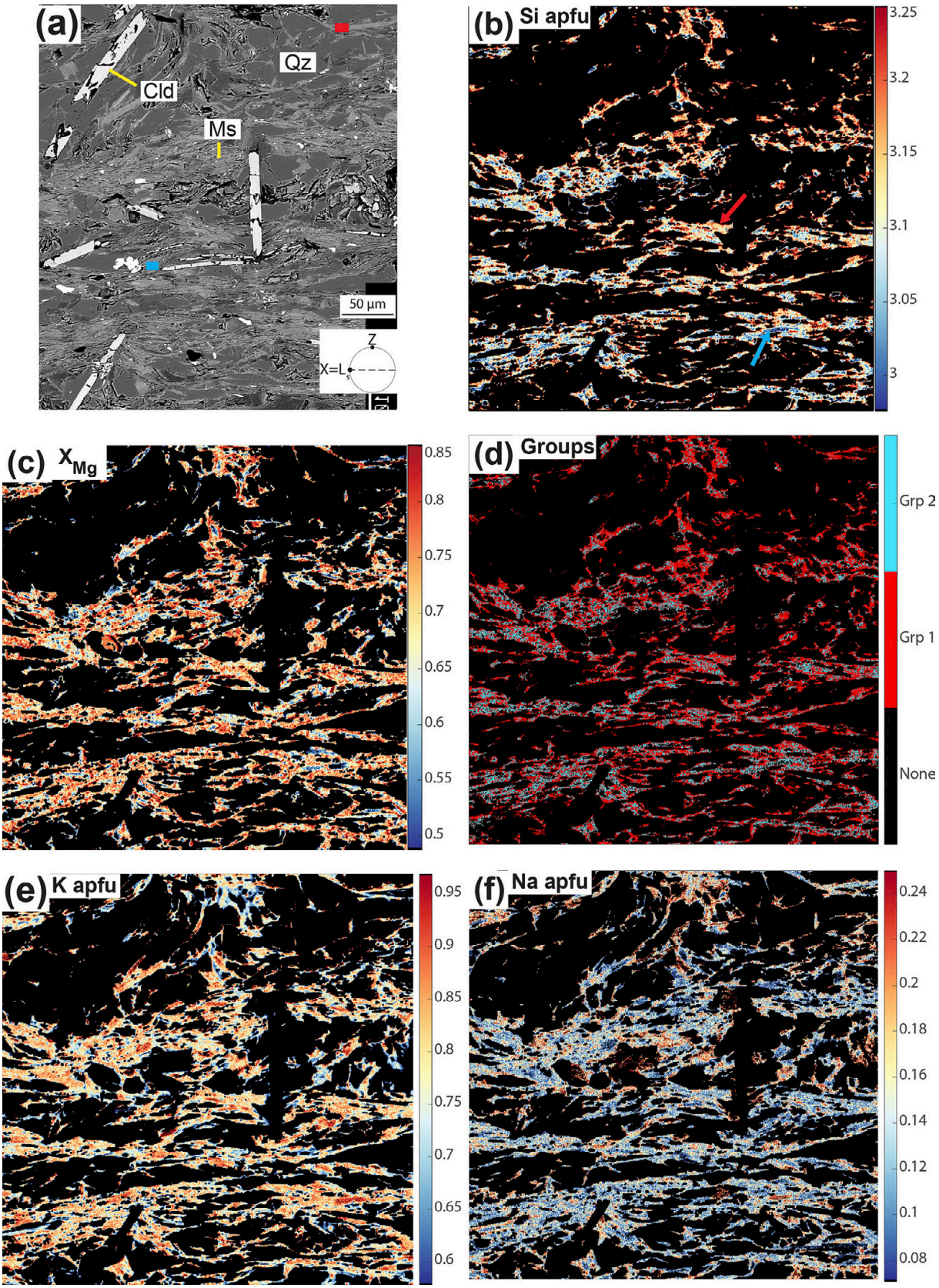

Fig. 5. (a) Backscattered electron image of metapelite sample FG1922 from the MRU. Note chloritoid and phengitic muscovite oriented both parallel and at high angle to the main foliation. Compare with Fig. 9 of Giuntoli and Viola (2021). Red and light blue rectangles refer to high and low Si apfu muscovite areas presented in Table 1. (b-f) X-ray compositional map of muscovite. (b) Si apfu, high and low Si contents shown by the red and light blue arrows, respectively. (c) X_{Mg} content. (d) Distinction in two groups based on the Si content (see text). (e) K apfu. (f) Na apfu. (For interpretation of the references to colour in this figure legend, the reader is referred to the web version of this article.)

Gaussian distribution of a single, homogeneous mica population. Additionally, the Si–(Al_{tot} + Mg + Fe) bivariate plot of the sample of the Island of Giglio displays instead a correlation with a break in slope at [Si] ≈ 3.1 (Supplementary Fig. 1a,b). A uniform slope would be interpreted as a sub-μm intergrowth of a low-Al-high-Si phengitic mica with a high-Al-low-Si muscovite (Supplementary Fig. 1e,f). The break in slope is caused by the addition of Mg and Fe as substituent cations for Al in the retrograde muscovite. This implies that the retrogression of phengite occurred in a chemically open system. Thus, at the scale of each μm EPMA spot, the mass balance of HP phengite, early retrograde muscovite, and late-stage retrograde muscovite is variable. The introduction of Cl, not directly measured in the present EPMA analyses, is a very likely side-effect of the open-system aqueous alteration. As discussed in § 4.3, the influence of a Cl-rich phase on Ar isotope systematics needs to be

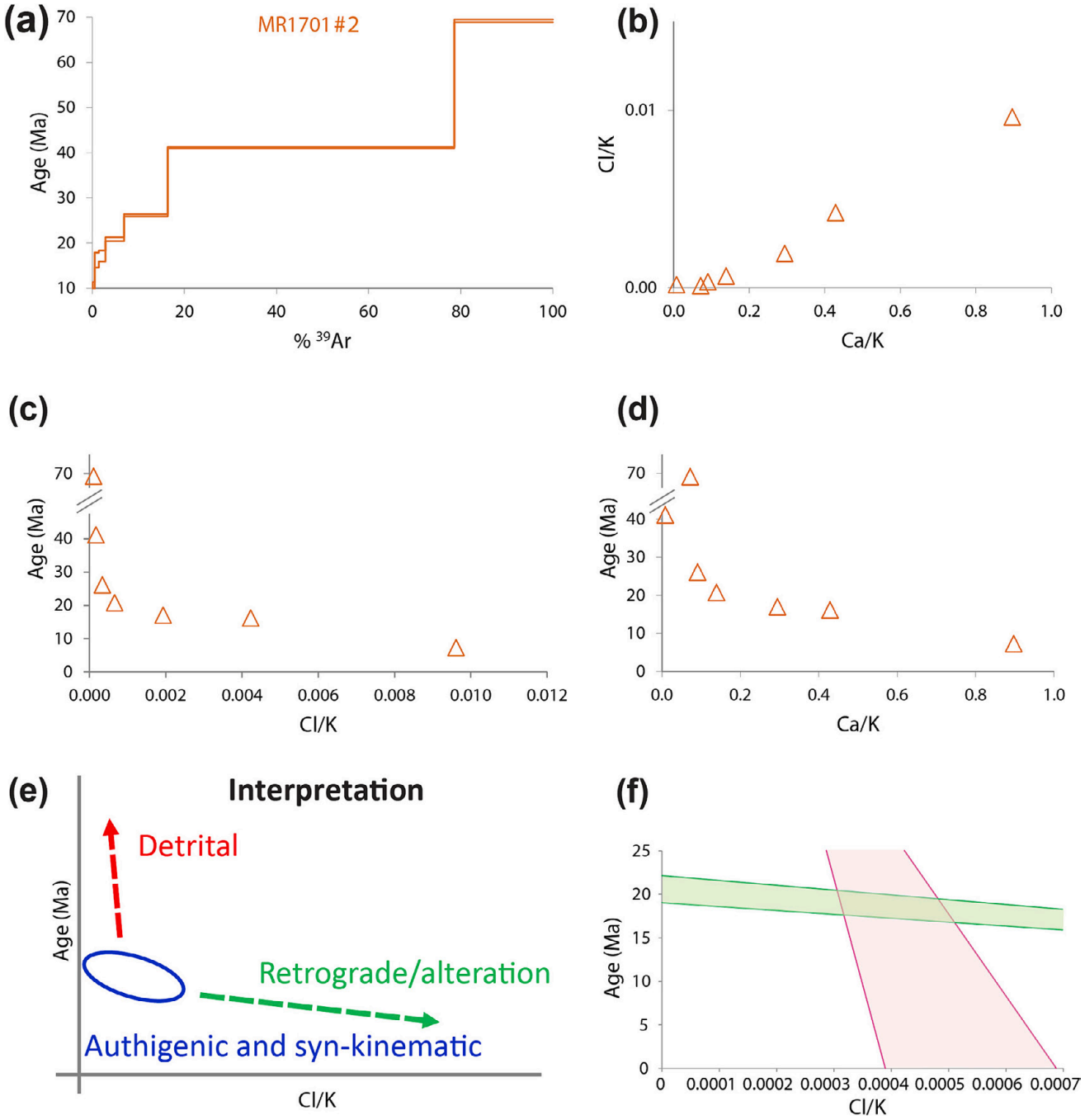

Fig. 6. Age data of fraction #2 of metarenite sample MR1701 from the MRU. (a) $^{40}Ar/^{39}Ar$ age spectra of muscovite. In the following images, fraction #1 is displayed by dots, and fraction #2 by triangles. (b) Cl/K versus Ca/K diagram. (c) The age versus Cl/K correlation diagram shows a decreasing age for increasing Cl/K. (d) The age versus Ca/K correlation diagram shows a negative correlation. (e) Interpretation of the age versus Cl/K correlation diagram. The green and red arrows denote the retrogression/alteration trend of the high-pressure neoblastic mica and the admixture of detrital mineral phases to the high-pressure neoblastic mica, respectively. (f) Detail of the intersection between the two coloured trend lines sketched in Fig. 6e. The light green shaded area represents the high-pressure neoblastic mica–alteration trend line, whose thickness corresponds to its analytical-only 1 sigma uncertainty. The pink shaded area represents the high-pressure neoblastic mica–detrital trend line, whose thickness is the analytical-only uncertainty. The intersection of the two trends, at Cl/K = 0.00035 ± 0.00005 and t = 20.1 ± 1.5 Ma, likely dates the crystallization of the metamorphic phengite. (For interpretation of the references to colour in this figure legend, the reader is referred to the web version of this article.)

examined in context with the microchemical data.

4.3. Age dating results and interpretation

Results are presented starting from the Monticiano-Roccastrada Unit, as we use sample MR1701 as a guide to interpret all the other samples. We assign little importance to, and do not discuss, the lowermost temperature steps that account for <<1 % of the total Ar release (see Table S2, where all steps are listed). In principle, these steps could be due to recoil artefacts; if this is the case, the Ca/K ratio should be lower than that of the sum of all steps, as ^{37}Ar has a longer recoil distance than ^{39}Ar and is more strongly depleted in a recoil-dominated artefact. Whenever this is not observed, a contribution from a Ca-rich contaminant phase is required. As this contaminant phase only contributes an almost negligibly small amount of Ar, its contribution to the general picture (the presence of retrograde phases) is almost negligible.

4.3.1. Monticiano-Roccastrada Unit (MRU)

Cl/K – age and Ca/K – age correlation diagrams of metaquartzarenite sample MR1701 (only fraction #2) display decreasing ages with increasing Cl/K and Ca/K ratios (Fig. 6). Both graphs show a triangle-shaped trend that reflects the mixture between the three phases mentioned in § 4.2: alteration phases, detrital phases, and newly formed (neoblastic and *syn*-kinematic) mica. The lowest ages (< 15 Ma) correspond to the highest Cl/K and Ca/K values and in the plot define a shallow negatively sloped trend (Fig. 6). This trend is interpreted as an admixture of small amounts of Cl-rich alteration phases with newly formed synkinematic mica. The oldest ages (defining a steeply increasing trend from 25 to 70 Ma) correspond to very low and decreasing Cl/K ratios, which indicates a progressively increasing contribution of detrital phases, probably feldspar, as it is practically the only K-rich and Cl-poor mineral. The strongly simplified assumption that purely analytical uncertainties need to be considered is made necessary by the fact that no systematic uncertainty on the number of detrital and alteration phases can be estimated. This simplified assumption provides a semiquantitative estimate of the age of the high-pressure mica, whose confidence interval is defined by the intersection of the two shaded areas that represent the alteration trend (with its analytical uncertainty) and the inheritance trend (with its analytical uncertainty; Fig. 6f). The resulting estimate of the high-pressure mica composition and age is Cl/K = 0.00035 ± 0.00005, Age = 20.1 ± 1.5 Ma. An estimate of the mass fraction of newly formed phengite can be based on the upper ordinate intercept of the steep trend, giving an apparent bulk age of the detrital feldspar (80 Ma), on the interpreted age of the pure mica, 20 Ma (see above), and on the integrated age of the entire sample (neglecting the small contribution of alteration phases). By cross-multiplication we calculate that 60 % of the total ^{39}Ar was contained in phengite and 40 % in detrital feldspar. It should be noted that the high original age of the detrital minerals (which lie in a Triassic sediment) causes them to contribute large amounts of inherited Ar even if their mass fraction is low.

The Cl/K – age and Ca/K – age correlation diagrams for metapelite sample FG1922 (only fraction #2) display a V-shaped trend like that of sample MR1701, with a decrease in ages correlating with an increase in Cl/K and Ca/K ratios (Fig. 7). Low Cl/K and Ca/K values are associated with ages between 140 and 25 Ma. We interpret them as resulting from mixing between the high-pressure neoblastic mica and Cl-poor detrital phases of unspecified age > 140 Ma. It is worth noting that individual step ages are due to a mixture and, thus, do not date the detritus. The highest Cl/K and Ca/K values correspond to ages <15 Ma and are, again, best interpreted as reflecting mixing between neoblastic mica and secondary retrograde/alteration phases. The intersection of the two trends at Cl/K = 0.0006 and *t* = 19–20 Ma would mark the age of the metamorphic phengite.

Cl/K – age and Ca/K – age correlation diagrams for metaquartzarenite sample FG1924 display different trends for fractions #1 (dots) and

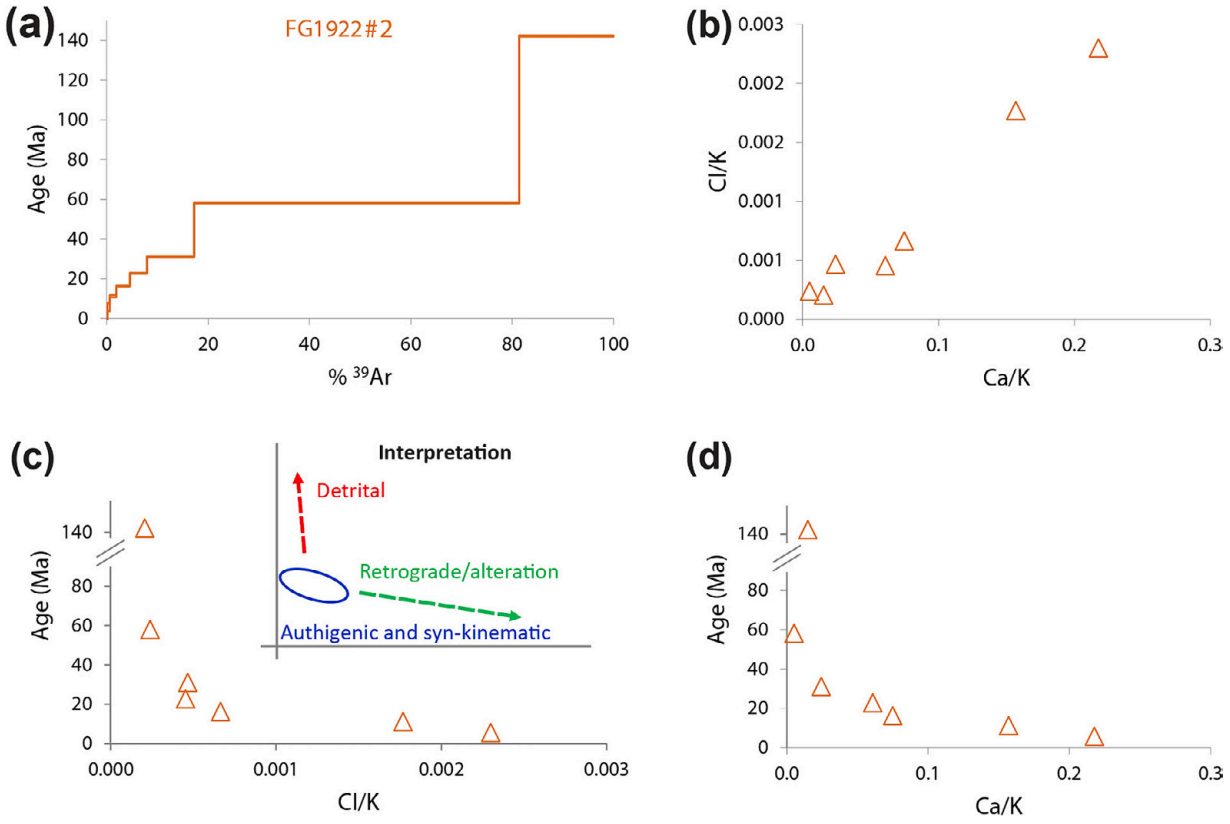

Fig. 7. Age data of fraction #2 of metapelite sample FG1922 from the MRU. (a) ^{40}Ar/^{39}Ar age spectra of muscovite. (b) Cl/K versus Ca/K diagram. (c) The age versus Cl/K correlation diagram shows a decreasing age for increasing Cl/K and interpretation. (d) The age versus Ca/K correlation diagram shows a negative correlation.

#2 (triangles; Fig. 8). Fraction #2 displays a similar trend to that from sample MR1701, with low Cl/K and Ca/K values corresponding to ages between 70 and 20 Ma and higher Cl/K and Ca/K values to ages of ca. 20 Ma. Fraction #1, instead, resembles a "V"-shaped trend, with low Cl/K and Ca/K values associated with ages between 48 and 20 Ma and then higher Cl/K and Ca/K values related to ages between 22 and 52 Ma. It is worth noting that both fractions intersect at ca. 20 Ma for low Cl/K and Ca/K values.

The Cl/K – age correlation diagram for metaquartzarenite sample FG1921 exhibits a similar trend for both fractions (Fig. 9). A cluster formed by steps with a low Cl/K has an age of 19 ± 2 Ma, which we interpret as the crystallization age of the metamorphic phengite. An increase in Cl/K and Ca/K values above 0.08 and 0.45, respectively, corresponds to an age increase up to ca. 70 Ma for both fractions.

In summary, samples from the Monticiano-Roccastrada Unit display mixing between three main components: low Cl/K and Ca/K values can be related to mixing between detrital Cl-poor phases, probably feldspar (s), and neoblastic mica. High Cl/K and Ca/K values are attributed to retrograde/alteration phases. All Cl/K and Ca/K ratio diagrams confirm that the radiogenic sources are at the very least three, as the data do not plot along a line. These data support an age of ca. 19 ± 2 Ma for the crystallization of phengitic muscovite (higher-[Si] content, i.e. blues-chist facies conditions), whereas ages between 15 and 11 Ma associated with the highest Cl/K and Ca/K ratios likely date the retrogression to greenschist facies conditions.

4.3.2. *Island of Giglio*

For the three samples from Island of Giglio the Cl/K vs. Ca/K compositional correlation plots (Figs. 10b, 11b, 12b) exhibit a "S"-shaped trend. This is evidence that in the Island of Giglio samples the required minimum number of major mixture endmembers is four. Accordingly, the Cl/K – age and Ca/K – age correlation diagrams display a "U"-shape (Figs. 10c,d, 11c,d 12c,d) unlike the V-shaped (three-component) trends of the MRU samples (Figs. 6c,d, 7c,d, 8c,d, 9c,d). This reflects an intrinsic property of these three samples, which feature low-temperature steps with high Cl/K ratios (indicative of alteration) and at the same time high apparent step ages. By analogy with the MRU samples, we interpret the intermediate temperature steps as the best constraint on the age of the newly formed synkinematic phengite.

Metapelite sample FG1940 shows a decrease in ages from 65 to 23 Ma for low Cl/K and Ca/K values (Fig. 10). Increasing Cl/K and Ca/K values to 0.02 relate to a decrease in age to 11.5 Ma. Higher Cl/K and Ca/K values relate to ages >25 Ma.

Cl/K – age and Ca/K – age correlation diagrams of metaquartzarenite sample FG1941 for both fractions display again a "U" trend, with a decrease in age to between 50 and 25–20 Ma for low Cl/K and Ca/K values (Fig. 11). Increasing Cl/K and Ca/K values to 0.02 correspond to a decrease in ages to 16 Ma. For Cl/K values >0.02 and 0.03 for Ca/K ages increase to 90 Ma.

Cl/K – age and Ca/K – age correlation diagrams of metapelite sample FG1942 (only fraction #1 analysed in two separate sessions named "first and second", respectively) display a "U" trend with a decrease in ages spanning between 65 and 24 Ma for low Cl/K and Ca/K values (Fig. 12). Increasing Cl/K and Ca/K values to 0.028 and 0.145, respectively, correspond to a decrease in ages from 18 to 15 Ma. For Cl/K values >0.03 and Ca/K > 0.15, ages increase to 45 Ma.

Summarizing, samples from the Island of Giglio represent a mixing between mineral endmembers produced by the same three geological

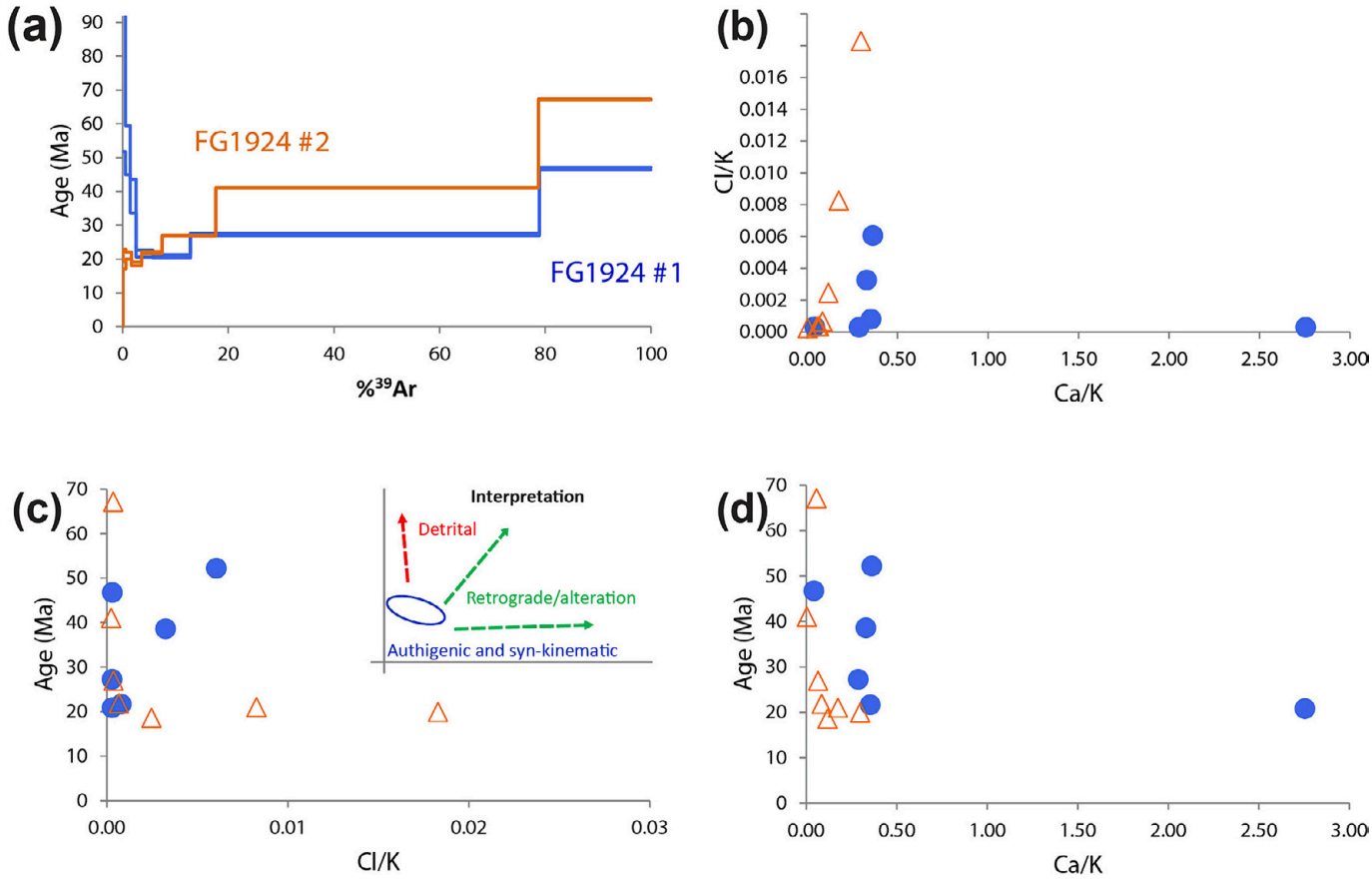

Fig. 8. Age data of fractions #1 (dots) and #2 (triangles) of metarenite sample FG1924 from the MRU. (a) $^{40}Ar/^{39}Ar$ age spectra of muscovite. (b) Cl/K versus Ca/K diagram. (c) The age versus Cl/K correlation diagram shows a decreasing age for increasing Cl/K for fraction #2 and a "V" shape for fraction #1 and interpretation. (d) The age versus Ca/K correlation diagram shows a similar trend to the previous graph.

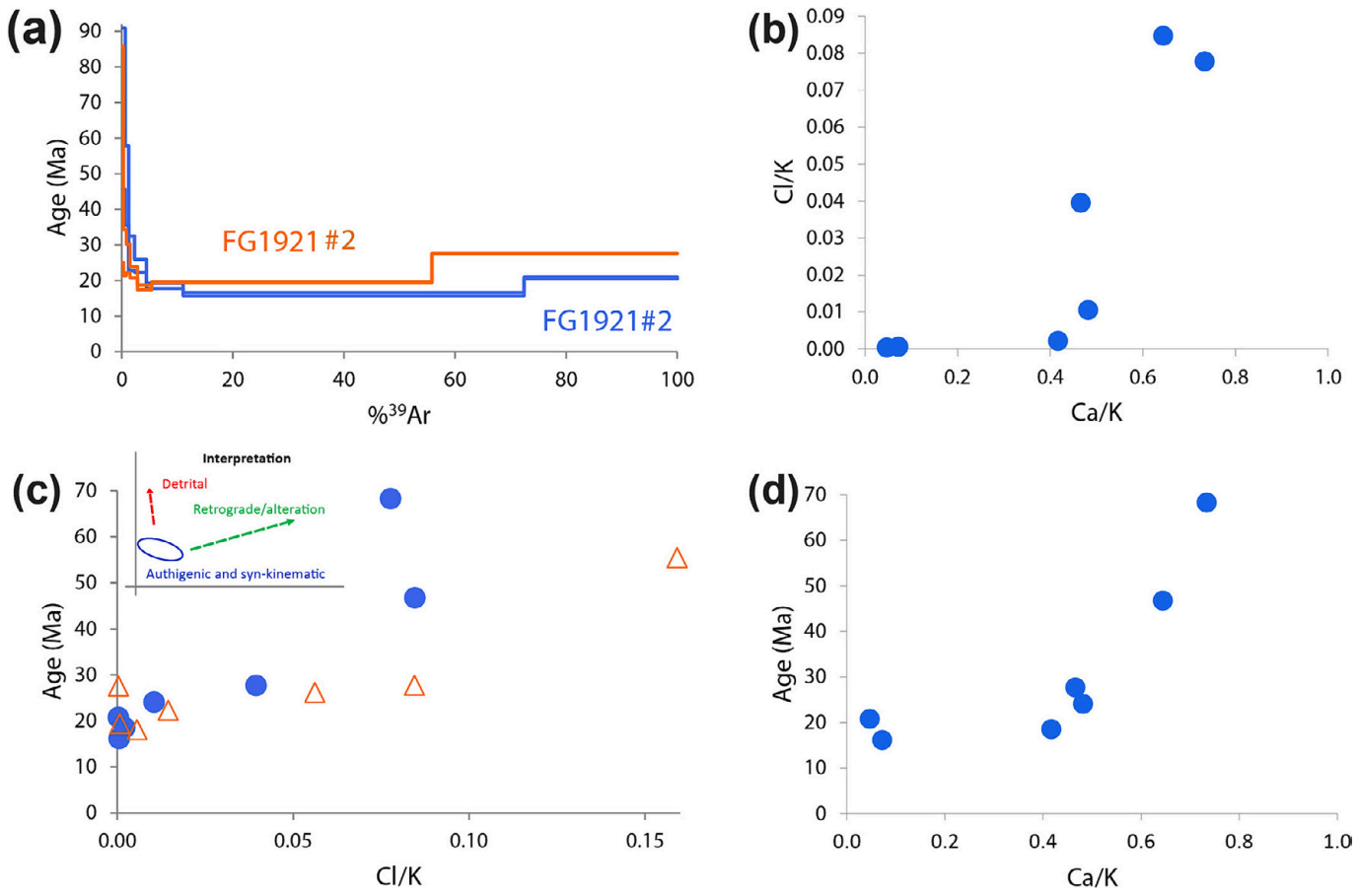

Fig. 9. Age data of fractions #1 and #2 of metarenite sample FG1921 from the MRU. (a) $^{40}Ar/^{39}Ar$ age spectra of muscovite. (b) Cl/K versus Ca/K diagram only for fraction #1, as the analysis of fraction #2 was performed after the pandemic, when $^{37}Ar_{Ca}$ was already decayed. (c) Age versus Cl/K correlation diagram shows a similar trend for both fractions and interpretation. (d) Age versus Ca/K correlation diagram shows a "U" trend.

processes identified for the Monticiano samples: preservation of detrital relict minerals, new formation of phengite under high-pressure (blueschist facies) conditions, and alteration. In the Island of Giglio samples alteration followed two separate trends, with at least two relict phases, bringing the total number of components to five. The exact number of mixing endmembers, which depends on the mineralogical composition of individual samples, is of secondary importance, as it does not change the petrological-geological observation that all the studied rocks record a three-stage evolution: (i) formation of a pre-metamorphic protolith, (ii) blueschist facies high pressure metamorphism, and (iii) retrograde reactions during exhumation. The very low Cl/K and Ca/K ratios and the very high outgassing temperature (much above the typical dehydration-related collapse of white mica) suggest the presence of sub-μm sized detrital feldspar. High Cl/K values in the low-temperature steps likely represent admixture of retrograde/alteration phases. These data support ages of ca. 18–16 Ma related to phengitic muscovite formation under blueschist facies conditions, whereas ages >20 Ma are interpreted as deriving from detrital phases. Ages of 15–11 Ma from the steps with higher Cl/K and Ca/K ratios likely date the retrogression to greenschist facies conditions.

We note that the qualitative trend in the age-vs-Cl/K and Ca/K correlation diagrams is the same for both sites. However, cross-multiplication between our hypothesized neoblastic phengite and the detrital phases yields a quite different mass balance: at Monticiano the neoformed mica is 50–60 % of the total, whereas on Island of Giglio it is only 20–30 %, and the detrital phases dominate over the phengite. High Cl/K values can be related to the alteration of neoblastic mica and growth of Cl-rich clay. High Ca/K values may be related to zeolites rich in Ca.

5. Discussion

5.1. Linking age data with meso- and microstructures and P-T constraints

On the Island of Giglio, Giuntoli and Viola (2022) constrained mylonitic foliation development to blueschist facies conditions at 1 GPa and ~350 °C. Later top-to-the E S-C/C′ structures were instead interpreted as constraining incipient retrogression to greenschist facies conditions (see Supplementary information of Giuntoli and Viola, 2022). Such a two-stage evolution is also reflected in muscovite composition at the microscale, with group 1 as per Fig. 4d associated with the blueschist facies foliation and group 2 related to retrograde conditions. We link, therefore, the 18–16 Ma age range to blueschist facies deformation, while the 15–11 Ma ages record retrogression to greenschist facies conditions.

For the MRU along the Farma River, Giuntoli and Viola (2021) reported that the duplex-related mylonitic fabric formed during blueschists facies top-to-the *E*-NE thrusting at 0.7–1.1 GPa and 350 °C–400 °C, followed by retrogression to greenschist facies conditions at the microscale, as documented by the lower [Si] content of muscovite of group 2 close to grain boundaries and pyrophyllite locally overgrowing carpholite (Fig. 5d). Therefore, we link the 21–17 Ma age range to blueschist facies fabric formation and the 15–11 Ma age range to retrogression to greenschist facies conditions.

These relatively broad age ranges could result from different processes. In both study areas, the maximum recorded deformation temperature is 400 °C, which excludes effective volume diffusion (e.g. Villa et al., 2014; Warren et al., 2012a). Apparent $^{40}Ar/^{39}Ar$ ages older than expected can be due to two opposed processes (Villa et al., 2014, p. 817).

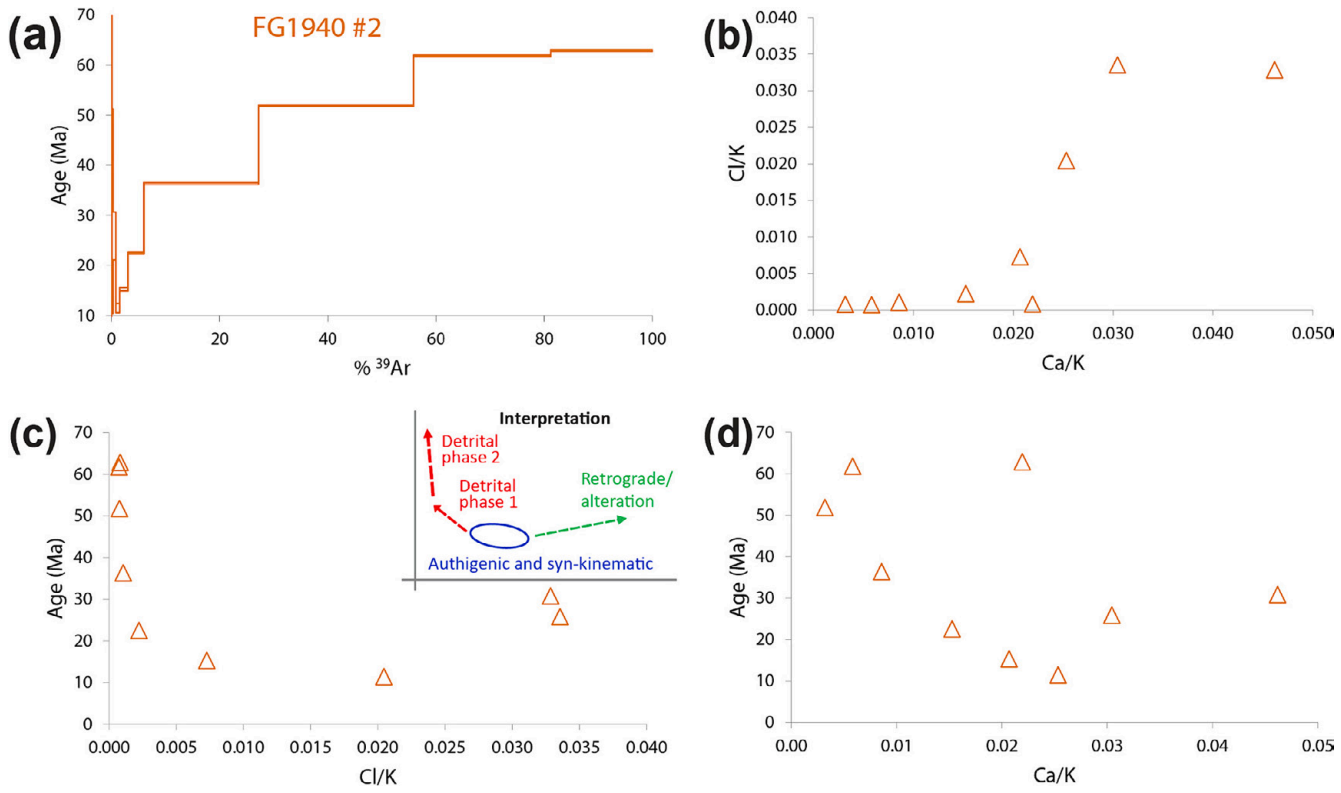

Fig. 10. Age data of fraction #2 of metapelite sample FG1940 from the Island of Giglio. (a) $^{40}Ar/^{39}Ar$ age spectra of muscovite. (b) Cl/K versus Ca/K diagram. (c) The age versus Cl/K correlation diagram shows a "U" trend and interpretation. (d) Age versus Ca/K diagram.

The first one, addition of "excess" ^{40}Ar by an external fluid, is excessively often invoked without unambiguous proof (such as had been provided by Rama et al., 1965). In fact, apparent "excess" Ar can be produced by alteration reactions (Chafe et al., 2014; Villa and Bosio, 2022), which are revealed by their devious Ca/K and/or Cl/K ratios as frequently observed in the lowest-temperature degassing steps. The second one, incomplete loss of radiogenic Ar from a precursor mineral phase, should be termed "inherited" Ar. In the present samples, excessively high ages are due both to (partial) Ar inheritance in relict (detrital) mineral phases degassed in the high-temperature steps and to minute (down to submicron in size) Cl-rich alteration phases degassed in the lowermost temperature steps (samples FG1924 fraction #1, FG1921 fraction #2, FG1940, FG1941 and FG1942). Note that detrital minerals, such as feldspar or white mica were not resolved at the microscopic scale in the present study. Nonetheless, detrital minerals can also occur at the sub-micron scale or as relicts at the core of neoblastic minerals. Notably, it is common for polydeformed terranes to contain multiple overprinting fabrics associated with repeated blastesis stages to produce often incomplete isotopic homogenization. Particularly in the case of polyphase deformation occurring under retrograde conditions, it is common to observe layer-by-layer retrograde substitution of phengite by muscovite causing fine intergrowths of the two (well below 10 μm), The size issue challenges and questions the use of laser ablation for in-situ dating (see Villa and Hanchar, 2017), as the laser beam is at least one order of magnitude larger than the size of the intergrown microstructures. Additionally, fluid circulation during retrograde metamorphism and exhumation may promote partial or pervasive white mica recrystallization and dissolution – precipitation processes, which, in turn, makes it very challenging to untangle the isotopic contribution of inheritance and neoblastic crystallization and leads to ages that reflect mixing of different tectono-metamorphic processes (e.g., Airaghi et al., 2018; Rolland et al., 2009; Warren et al., 2012b).

These different processes require work-intensive protocols to date polyphase white mica by $^{40}Ar/^{39}Ar$ (Mulch et al., 2005; Villa et al., 2014), or by combined Rb—Sr and $^{40}Ar/^{39}Ar$ (Villa et al., 2023). It is well known (Foland, 1983; Hodges et al., 1994; Villa et al., 2014, p. 821) that age spectra exhibiting "plateaus" can be geologically meaningless artefacts due to simultaneous degassing of different mica generations. Therefore, a more thorough approach that links chemical information with the degassing spectra should be pursued to depict the mixing of two or more components, such as the common denominator three-isotope correlation diagrams used in the present study.

We have petrological evidence that in our samples the high-pressure phengitic muscovite was partially replaced by lower pressure muscovite, as shown by the mica compositional maps (Figs. 4 and 5). Nonetheless, by using the approach of common denominator three-isotope correlation diagrams we were able to disentangle the contribution of the different components, thus excluding (or limiting) the likelihood of misinterpreting mixed ages as genuine end-member ages (e.g. Villa et al., 2023). In fact, the obtained broad age ranges could also reflect the duration of protracted deformation during retrograde conditions, as recently proposed for the Apennines (Di Vincenzo et al., 2022) and for other collisional settings (e.g. Giuntoli et al., 2020; Montemagni et al., 2019; Viola et al., 2011; Walters and Kohn, 2017). We suggest that the age ranges that we extracted from our samples likely reflect the duration of thrusting.

5.2. *Comparison with previous geochronological data and related pressure-temperature constraints*

A summary of published age data for the Northern Apennines is provided in Table 2. The most reliable estimates of the age of the blueschist event require a petrochronological approach, as all the samples from the Northern Apennines exhibit a complex petrogenesis. Several of the legacy works from the 1970s and 1980s use the now discontinued K—Ar bulk dating technique, whose results have been considered unreliable for the past 30 years. Even later papers presenting $^{40}Ar/^{39}Ar$ age determinations do not always supply a context between

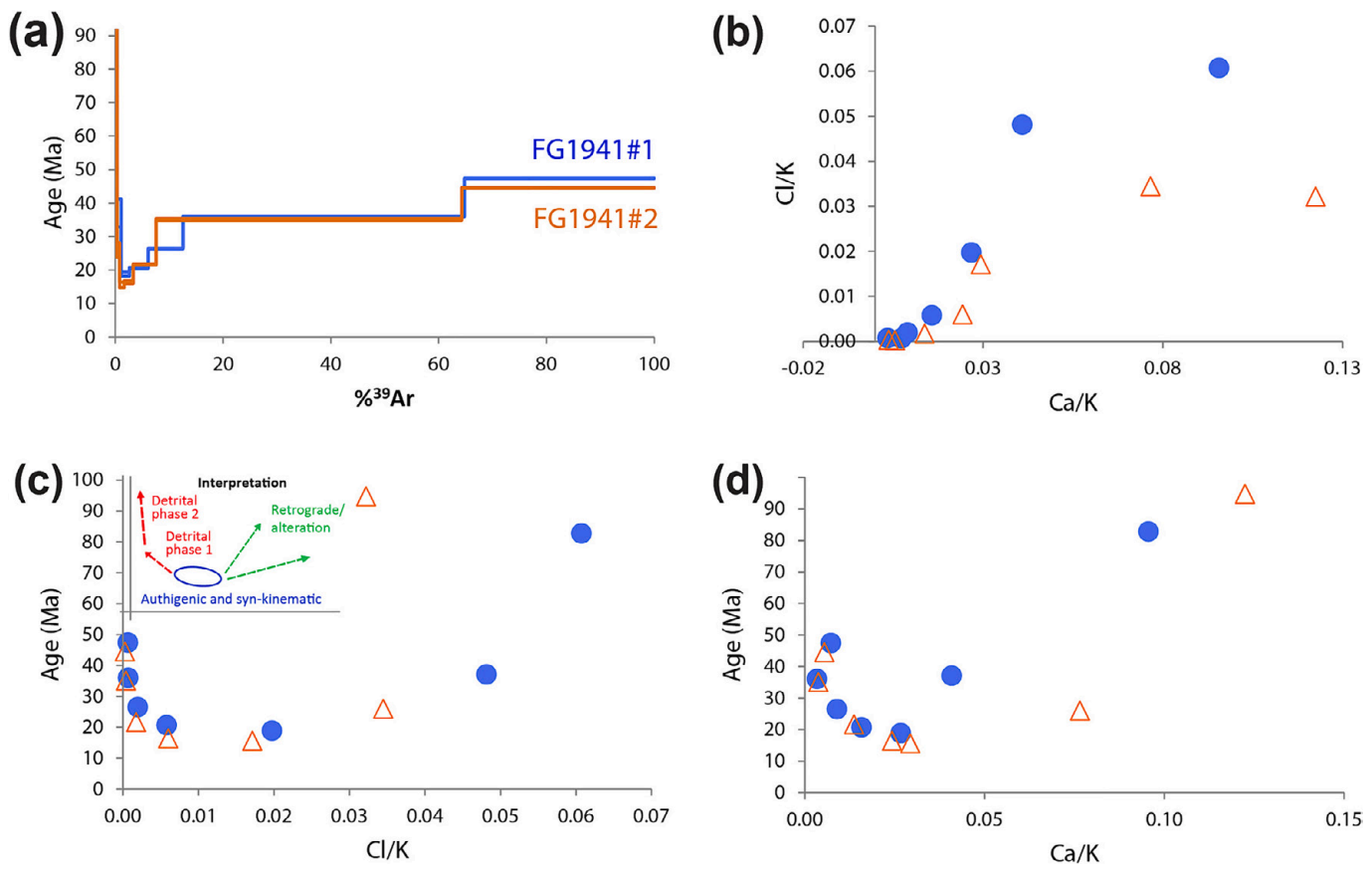

Fig. 11. Age data of fractions #1 and #2 of metarenite sample FG1941 from the Island of Giglio. (a) $^{40}Ar/^{39}Ar$ age spectra of muscovite. (b) Cl/K versus Ca/K diagram. (c) Age versus Cl/K correlation diagram shows a similar "U" trend for both fractions and interpretation. (d) Age versus Ca/K correlation diagram.

the microstructural and compositional constraints needed to discriminate among the multiple mineral generations (relict, peak metamorphic, retrograde) and the isotope analyses. Moreover, the data reporting is not always complete, which prevents an independent assessment of the reliability of the inferred ages. The Ar isotopic data always needed are the absolute concentration data for all five isotopes, to allow for both the stoichiometric control and the recognition of Ca/Cl/K fingerprints of the different mineral generations. A critical review of legacy papers was performed by Di Vincenzo et al. (2022). Below, we mention these age data, starting from more internal to external areas of the Northern Apennines (from W-SW to *E*-NE); readers should keep in mind that these legacy papers do not always provide insight on the multiple phases of a multistage geological history.

At the Island of Gorgona, the high-pressure stage of ca. 1.5 GPa and 350 °C was dated to~25 Ma (Brunet et al., 2000; Rossetti et al., 2001). Retrogression to ~0.5 GPa and ~300 °C was proposed as occurring there at ~18 Ma, although this stage is less reliably constrained (age data from Brunet et al., 2000 and P-T data fromJolivet et al., 1998; Rossetti et al., 2001). At the Island of Elba, the high-pressure stage of 1.5 GPa and ~480 °C was dated to ~20 Ma (age data from Bianco et al., 2019; Deino et al., 1992 and P-T from the former). A similar age range of 21–19 was related to deformation occurring at ~1.5–1.8 GPa and 320–370 °C (age data from Ryan et al., 2021 linked to P-T from Papeschi et al., 2020).

No $^{40}Ar/^{39}Ar$ age data for the Island of Giglio are available in literature. Therefore, our age ranges of 18–16 Ma for deformation occurring at >1 GPa and ca. 350 °C and 15–11 Ma for retrograde conditions are the first age constraints for the locality. Balestrieri et al. (2011) interpreted zircon fission tracks of ca. 30 Ma for the Island of Elba and ca. 18 Ma for the Island of Giglio as related to cooling after peak metamorphism but assigned it an unrealistically low temperature of <200–180 °C (Tagami et al., 1998) and do not model track lengths as a function of the exhumation history, as the recent evolution of fission track studies would recommend (Malusà and Fitzgerald, 2019). Therefore, these ages seem old compared to existing literature data from adjacent areas and to the maximum depositional age of metasedimentary sequences on the Island of Elba (Jacobs et al., 2018). Similarly, the ZFT ages of ca. 18 Ma for the Island of Giglio are nearly contemporaneous with the HP event constrained in this study.

For the Alpi Apuane region, Kligfield et al. (1986) proposed Oligocene K—Ar and $^{40}Ar/^{39}Ar$ ages for the peak metamorphic conditions, and Miocene ages for the retrograde conditions and the final, post-tectonic cooling. Miocene K—Ar ages were also reported by Giglia and Radicati di Brozolo (1970) and Radicati di Brozolo and Giglia (1973). Abbate et al. (1994) and Fellin et al. (2007) addressed the latest exhumation stage, after the termination of metamorphism, by zircon and apatite fission tracks and (U—Th)/He zircon and apatite ages between ca. 10 and 2 Ma. Most of these legacy papers provide coarse constraints on unresolved mixtures of petrogenetic phases, and/or more precise constraints on the latest stage of the post-metamorphic exhumation. In contrast, dating the high-pressure deformation events requires a careful disentangling of the petrological meaning of successive mineral generations. Recently, Di Vincenzo et al. (2022) constrained D1 structures to an age range of ca, 21–14.4 Ma in the Massa and Apuane units, reflecting a possible diachronism with the regional decreasing age trend from W to E. This stage was linked with P-T conditions of ca. 0.4–1 GPa and 250–500 °C (Molli et al., 2000) and with *syn*-contractional early exhumation. The same authors constrained D2 deformation to retrograde conditions around ca. 12.5–10.5 Ma for the entire Alpi Apuane region, with deformation representing the switch from contraction to extensional exhumation.

At the Argentario Promontory the chronology of high-pressure metamorphism and retrogression, (ca. 0.8 GPa and 350 °C and ca. 0.4

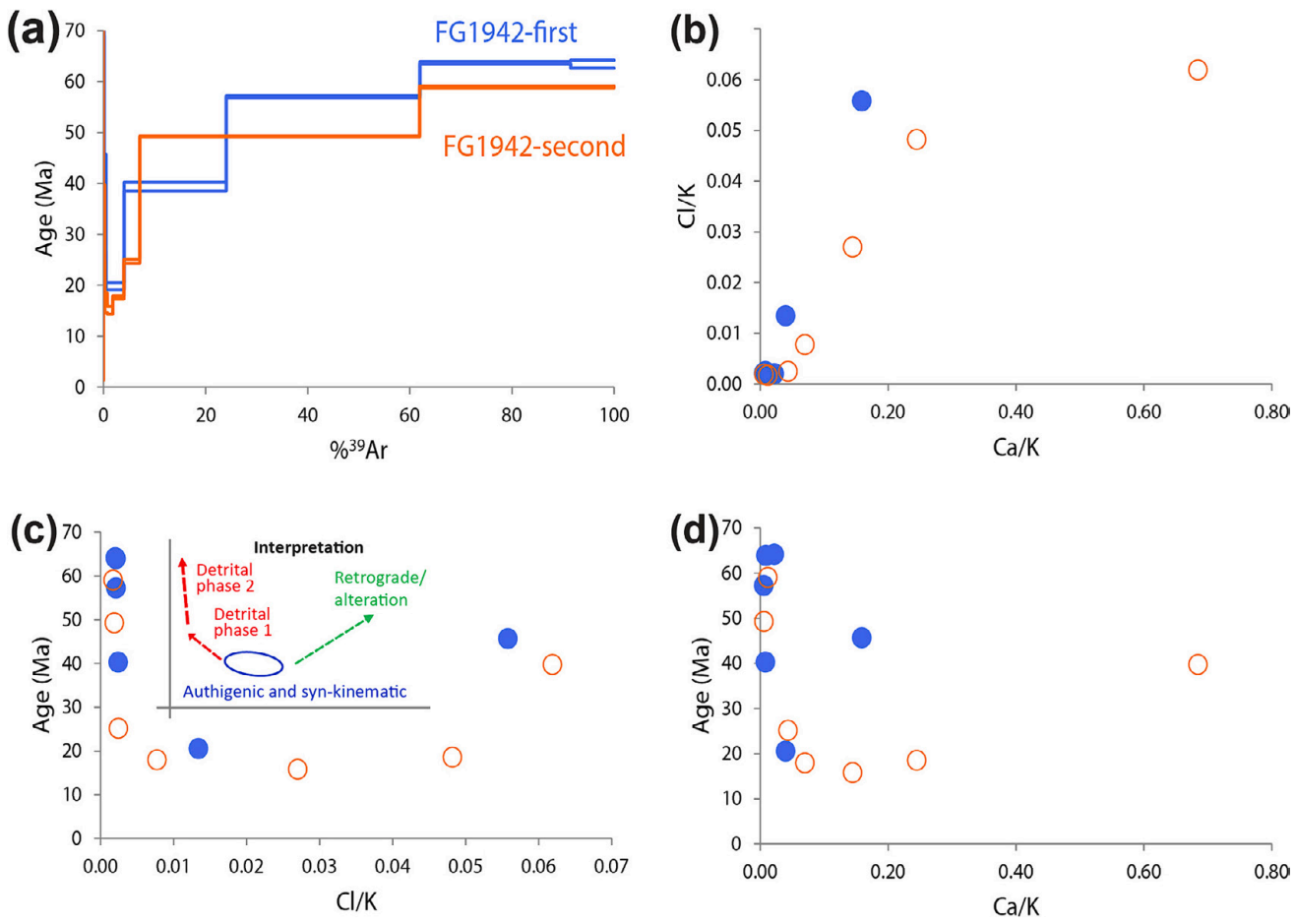

Fig. 12. Age data of fraction #1 (analysed in two separate sessions, "first" and "second", respectively) of metapelite sample FG1942 from the Island of Giglio. (a) $^{40}Ar/^{39}Ar$ age spectra of muscovite. (b) Cl/K versus Ca/K diagram. (c) Age versus Cl/K correlation diagram shows a "U" trend and interpretation. (d) Age versus Ca/K correlation diagram.

GPa and 350 °C, respectively, Theye et al., 1997) and exhumation was not well constrained (as discussed above); age estimates range from the Oligocene to the Pliocene (Balestrieri et al., 2011; Brunet et al., 2000).

For the high-pressure deformation in the Monticiano-Roccastrada Unit our age range represents the first age constraints for the area. The older age range of 21–17 Ma dates cyclic brittle and ductile deformation occurring at 0.7–1.1 GPa and 350–400 °C and the younger age range of 15–11 Ma incipient retrogression at greenschist facies conditions related to exhumation.

5.3. Geodynamic implications and exhumation of the high-pressure units of the Northern Apennines

In the literature, opposite end-member processes have been proposed for the exhumation of the high-pressure units of the Northern Apennines. In a first scenario, low-angle normal faulting is accounted for as the main mechanism leading to exhumation, whereby high-pressure units would have experienced syn-orogenic exhumation to shallow structural levels by top-to-the E low-angle detachment shearing. Geothermal gradients remained low during exhumation due to underthrusting of cold Adriatic units at depth (Brunet et al., 2000; Carmignani et al., 1994; Jolivet et al., 1998; Rossetti et al., 1999, 2002). Evidence of such low-angle normal shearing is reported from the islands of Gorgona and Giglio, where greenschist facies top-to-the E/SE ductile shear zone have been interpreted as detachment faults (Jolivet et al., 1998; Rossetti et al., 2001). However, recent studies have reconsidered the role of exhumation by normal faulting, proposing that this process can accommodate exhumation of only a few km. This would make the process responsible for only relatively minor exhumation and not for complete exhumation from several tens of km in the subduction channel (>40 km;Molli et al., 2018a; Musumeci et al., 2015).

An alternative scenario proposes that syn-collisional exhumation at high-pressure conditions occurred by an interplay of out-of-sequence thrusting, syn-orogenic extrusion and in-sequence thrusting. At the Island of Elba, Ryan et al. (2021) proposed syn-collisional exhumation by extrusion of the local Tuscan high-pressure Metamorphic Unit, the Acquadolce Subunit, based on the presence of top-to-the W extensional shear fabrics under retrograde blueschist facies conditions. In the Alpi Apuane region, the thrust that superposed the Massa Unit onto the Apuane Unit (belonging to the Tuscan Metamorphic Units) during retrograde high-pressure conditions was interpreted as a stage of syn-collisional exhumation (Molli et al., 2000, 2018b). Giuntoli and Viola (2021) proposed that the high-pressure contractional fabrics of the Massa Unit and the MRU may represent the deepest tectonometamorphic structures preserved in the Northern Apennines, which would record the onset of syn-orogenic exhumation still within the subduction channel. Comparing our new $^{40}Ar/^{39}Ar$ age data with comparable results by Di Vincenzo et al. (2022) we can advocate that the thrust superposing the Massa Unit onto the Apuane Unit and the duplex in the MRU are coeval. Moreover, similar age ranges also now emerge for the retrogression to greenschist facies conditions in the two units. Therefore, these contractional structures may represent the basis of the extrusion wedge proposed by Ryan et al. (2021), thus recording top-to-the E blueschist facies contractional fabrics coevally to the top-to-the W extensional shearing fabrics described on the Island of Elba.

In summary, we propose a refined exhumation history for the high-

Table 2
Summary of P-T-t data from the Ligurian Metamorphic Units (LMU) and Tuscan Metamorphic Units (TMU) of the Northern Apennines subdivided by locality. This table contains all published data, including those not amenable to a petrochronological approach, i.e. those which do not consider the microstructural and compositional constraints on multiple mineral generations and/or do not contain concentration data for all five Ar isotopes (see also paragraph 5.2).

Authors	Geological Unit	Location	Age Ma	P-T	Method	Mineral	Notes
Brunet et al., 2000	LMU	Gorgona Island	~25	~1.5 GPa and ~350 °C	$^{40}Ar/^{39}Ar$	White mica	Novel age data linked with P-T data from literature. See Fig. 13 of their manuscript.
Brunet et al., 2000	LMU	Gorgona Island	~18?	~0.5 GPa and ~300 °C	$^{40}Ar/^{39}Ar$	White mica	Novel age data linked with P-T data from literature. See Fig. 13 of their manuscript.
Rossetti et al., 2001	LMU	Gorgona Island	~25	~1.5 GPa and < 350 °C	$^{40}Ar/^{39}Ar$	White mica	
Balestrieri et al., 2011	TMU	Island of Elba, Rio Marina-Cavo	~30	Cooling after peak metamorphism	Fission-track	Zircon	Zircon minimum age
Deino et al., 1992	TMU, Ortano-Rio Marina	Island of Elba, Rio Marina	19.7 ± 0.5	Age data coeval with metamorphism of the unit	$^{40}Ar/^{39}Ar$	White mica	
Bianco et al., 2019	TMU, Continental Unit 2	Island of Elba, Rio Marina	19.8 ± 1.4	1.5 GPa and ~480 °C	$^{40}Ar/^{39}Ar$	Glaucophane	All five Ar isotopes reported
Ryan et al., 2021	TMU, Acquadolce	Island of Elba, Rio Marina	19–21	~1.5–1.8 GPa and 320–370 °C	$^{40}Ar/^{39}Ar$	White mica	Novel age date linked with P-T data from Papeschi et al., 2020; all five Ar isotopes reported
Balestrieri et al., 2011	TMU	Island of Giglio, Promontorio Franco	~18	Cooling after peak metamorphism	Fission-track	Zircon	Zircon minimum age
This Study	**TMU**	**Island of Giglio, Promontorio Franco**	**16–18**	**1 GPa and ~350 °C**	**$^{40}Ar/^{39}Ar$**	**White mica**	**Novel age data linked with P-T data from Giuntoli and Viola, 2022; all five Ar isotopes reported & compositional map of dated fabrics**
This Study	**TMU**	**Island of Giglio, Promontorio Franco**	**15–11**	**Retrograde conditions**	**$^{40}Ar/^{39}Ar$**	**White mica**	**Novel age data linked with P-T data from Giuntoli and Viola, 2022; all five Ar isotopes reported & compositional map of dated fabrics**
Giglia and Radicati di Brozolo, 1970	TMU	Alpi Apuane	~14–11	Final metamorphic stage, from W to E	K-Ar	White mica	
Radicati di Brozolo and Giglia, 1973	TMU	Alpi Apuane	~14–11	Final metamorphic stage, from W to E	K-Ar	White mica	
Kligfield et al., 1986 and Carmignani and Kligfield, 1990	TMU	Alpi Apuane	25–27	Peak metamorphic conditions	K-Ar and $^{40}Ar/^{39}Ar$	White mica	D1 compressive deformation phase
Kligfield et al., 1986 and Carmignani and Kligfield, 1990	TMU	Alpi Apuane	12–14	Retrograde conditions	K-Ar and $^{40}Ar/^{39}Ar$	White mica	D2 extensional deformation phase
Kligfield et al., 1986 and Carmignani and Kligfield, 1990	TMU	Alpi Apuane	8–10	Post tectonic cooling	K-Ar and $^{40}Ar/^{39}Ar$	White mica	Post tectonic cooling
Abbate et al., 1994	TMU	Alpi Apuane	6–2	<~120 °C	Fission-track	Apatite	
Brunet et al., 2000	TMU	Alpi Apuane	~25	~1 GPa and ~450 °C	$^{40}Ar/^{39}Ar$	White mica	Existing P-T-t data interpreted by the author. See Fig. 13 of their manuscript.
Brunet et al., 2000	TMU	Alpi Apuane	~14–11	~0.4–0.5 GPa and ~200–350 °C	$^{40}Ar/^{39}Ar$	White mica	Existing P-T-t data interpreted by the author. See Fig. 13 of their manuscript.
Fellin et al., 2007	TMU	Alpi Apuane	~10	Termination of metamorphism and ductile deformation	Fission-track	Zircon	
Fellin et al., 2007	TMU	Alpi Apuane	5.5 ± 0.9	<180 °C	He	Zircon	
Fellin et al., 2007	TMU	Alpi Apuane	4.7 ± 1.1	<~120 °C and < ~70 °C	Fission-track & He	Apatite	
Di Vincenzo et al., 2022	TMU	Alpi Apuane	~20–21-14.4	~0.4–1 GPa and ~350–500 °C	$^{40}Ar/^{39}Ar$	White mica	D1, possible diachronism with younging from W to E. Link with P-T data from Molli et al., 2000; all five Ar isotopes reported
Di Vincenzo et al., 2022	TMU	Alpi Apuane	~12.5–10.5	Retrograde conditions<~0.4 GPa and < ~350 °C	$^{40}Ar/^{39}Ar$	White mica	D2, link with P-T data from Molli et al., 2000; all five Ar isotopes reported
Brunet et al., 2000	TMU	Monte Argentario	~25	~0.8 GPa and ~380 °C	$^{40}Ar/^{39}Ar$	White mica	Novel age data linked with P-T data from literature. See Fig. 13 of their manuscript.

(*continued on next page*)

Table 2 (*continued*)

Authors	Geological Unit	Location	Age Ma	P-T	Method	Mineral	Notes
Brunet et al., 2000	TMU	Monte Argentario	~16	~0.4 GPa and ~380 °C	$^{40}Ar/^{39}Ar$	White mica	Novel age data linked with P-T data from literature. See Fig. 13 of their manuscript.
Balestrieri et al., 2011	TMU	Monte Argentario-Monti Pisani	6.1 ± 1.8	Cooling after peak metamorphism	Fission-track	Zircon	Zircon minimum age
Balestrieri et al., 2011	TMU	Monti dell'Uccellina	~27	Cooling after peak metamorphism	Fission-track	Zircon	Zircon minimum age
This Study	**TMU**	**Monticiano-Roccastrada**	**19 ± 2**	**>0.7 GPa and ~400 °C**	**$^{40}Ar/^{39}Ar$**	**White mica**	**Novel age data linked with P-T data from Giuntoli and Viola, 2021; all five Ar isotopes reported & compositional map of dated fabrics**
This Study	**TMU**	**Monticiano-Roccastrada**	**15–11**	**Retrograde conditions**	**$^{40}Ar/^{39}Ar$**	**White mica**	**Novel age data linked with P-T data from Giuntoli and Viola, 2021; all five Ar isotopes reported & compositional map of dated fabrics**

pressure metamorphic units of the Northern Apennines, integrating our new results with what has been proposed in the literature (Fig. 13; Brogi and Giorgetti, 2012; Giuntoli and Viola, 2021; Keller and Pialli, 1990; Molli et al., 2000, 2018a; Montomoli et al., 2009; Papeschi et al., 2020; Ryan et al., 2021; Storti, 1995). We relate ages of 21–16 Ma to blueschist facies conditions at 1 GPa and ~350 °C in high-pressure metamorphic units of the Northern Apennines. This older age range would mark either the deepest metamorphic conditions reached by the units or the beginning of the onset of syn-orogenic exhumation (Fig. 13a). Exhumation from blueschist facies conditions to greenschist facies conditions occurred by an interplay of out-of-sequence thrusting, syn-orogenic extrusion and in sequence thrusting in the age range of 15–11 Ma (Fig. 13b). High- and low-angle (e.g. those producing the "Serie Ridotta") normal faulting was active at shallower depths of the orogenic wedge and was responsible for exhumation in the last few kilometres (Molli et al., 2018a; Musumeci et al., 2015).

6. Conclusions

Our study provides new $^{40}Ar/^{39}Ar$ age constraints for two areas located at the western and eastern edges of the Tuscan Metamorphic Units of the Northern Apennines. At the Island of Giglio cyclic brittle and ductile deformation occurred at blueschist facies conditions of 1 GPa and ~350 °C around 18–16 Ma. In the Monticiano-Roccastrada Unit blueschist facies brittle and ductile fabrics associated with a duplex formed at 0.7–1.1 GPa and 350–400 °C around 21–16 Ma. Both areas experienced retrogression to greenschist facies conditions around 15–11 Ma.

Concluding, integrating our results with existing data, we propose that between 21 and 16 Ma the Tuscan Metamorphic Units experienced

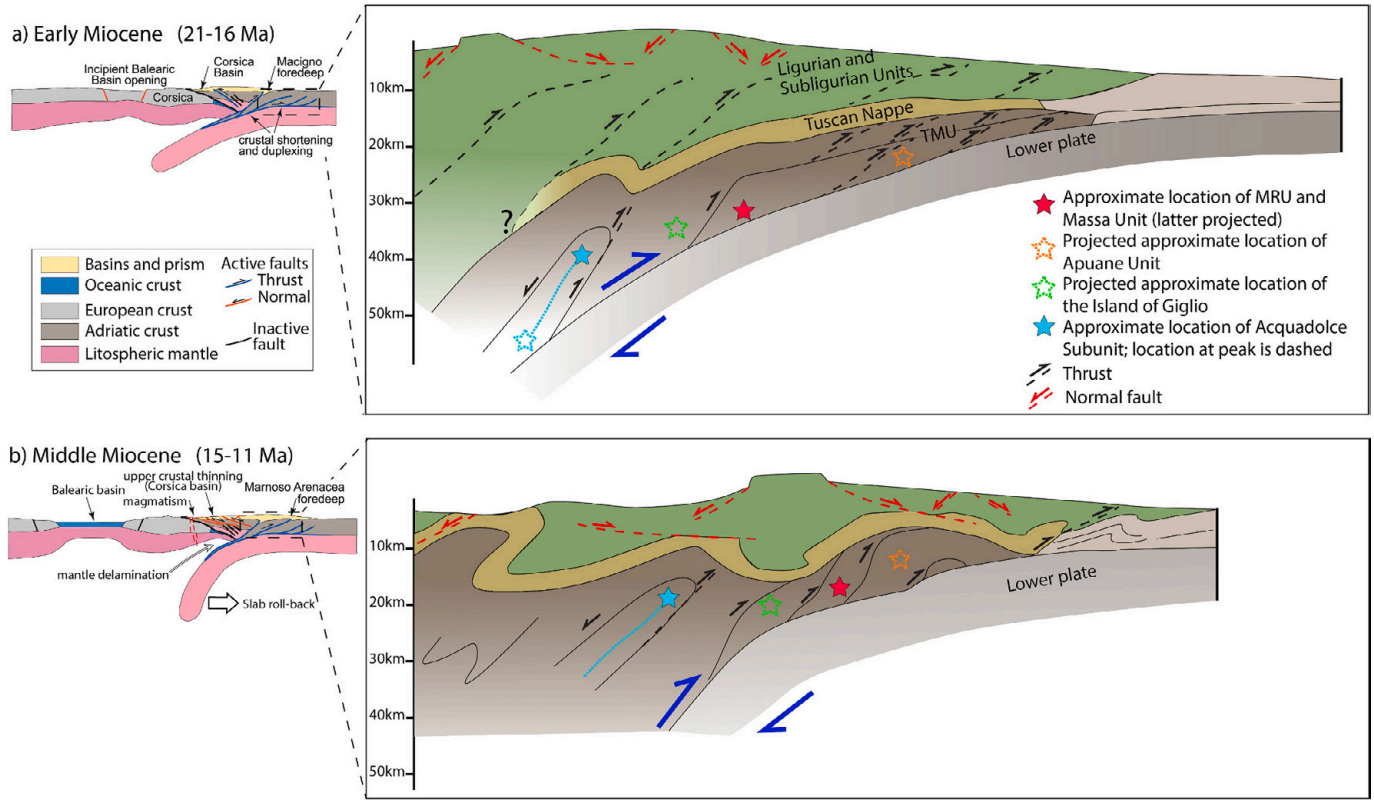

Fig. 13. Tectonic sketch of subduction in the Corsica-Northern Apennines belt with explicit focus on the tectonic setting of peak conditions of the Tuscan Metamorphic Units (a) and their exhumation to shallower structural levels (b) due to extrusion, out- and in-sequence thrusting. Sketches on the left modified from Bonini et al. (2014), on the right based on Molli et al. (2018b) and Ryan et al. (2021).

deformation at blueschist facies conditions (~1 GPa and 350 °C) marking the onset of syn-orogenic exhumation by a combination of extrusion, with underthrusting and top-to-the-east compressional setting associated with coeval top-to-the-west extensional, out-of-sequence thrusting and in sequence thrusting. The younger age range of 15–11 Ma marks exhumation to shallower structural settings and retrogression to greenschist facies conditions.

Supplementary data to this article can be found online at https://doi.org/10.1016/j.lithos.2024.107801.

CRediT authorship contribution statement

Francesco Giuntoli: Writing – review & editing, Writing – original draft, Visualization, Validation, Resources, Methodology, Investigation, Funding acquisition, Formal analysis, Data curation, Conceptualization. **Giulio Viola:** Writing – review & editing, Writing – original draft, Investigation, Conceptualization. **Igor M. Villa:** Writing – review & editing, Writing – original draft, Visualization, Methodology, Investigation.

Declaration of competing interest

The authors declare that they have no known competing financial interests or personal relationships that could have appeared to influence the work reported in this paper.

Acknowledgments

Valentina Barberini is warmly acknowledged for laboratory assistance. Fabio Gamberini is acknowledged for preliminary sample preparation. Stefano Poli and Andrea Risplendente are thanked for the EPMA data acquisition. We acknowledge constructive reviews from Giancarlo Molli and an anonymous reviewer. Nadia Malaspina is acknowledged for editorial handling.

This project has received funding from the European Union's Horizon 2020 research and innovation programme under the Marie Skłodowska-Curie grant agreement N° 839779.

References

Abbate, E., Balestrieri, M.L., Bigazzi, G., Norelli, P., Quercioli, C., 1994. Fission track datings and recent rapid denudation in Northern Apennines. Mem. Soc. Geol. It 48, 579–585.

Airaghi, L., Warren, C.J., de Sigoyer, J., Lanari, P., Magnin, V., 2018. Influence of dissolution/reprecipitation reactions on metamorphic greenschist to amphibolite facies mica 40Ar/39Ar ages in the Longmen Shan (eastern Tibet). J. Metamorph. Geol. 36, 933–958. https://doi.org/10.1111/jmg.12420.

Aldinucci, M., Brogi, A., Spina, A., 2008. Middle-Late Permian sporomorphs from the Farma Formation (Monticiano-Roccastrada Ridge, southern Tuscany): new constraints for the tectono-sedimentary history of the Tuscan Domain. Stratigraphy and palaeogeography of late-and post-Hercynian basins in the Southern Alps, Tuscany and Sardinia (Italy). Ital. J. Geosci. (Boll Soc Geol It) 127, 581–597.

Allaz, J., Engi, M., Berger, A., Villa, I.M., 2011. The effects of retrograde reactions and of diffusion on 39Ar-40Ar ages of micas. J. Petrol. 52, 691–716. https://doi.org/10.1093/petrology/egq100.

Azzaro, E., Cocozza, T., Di Sabatino, B., Gasperi, G., Gelmini, R., Lazzarotto, A., Sabatino, B., Gasperi, G., Gelmini, R., Lazzarotto, A., 1976. Geology and Petrography of the Verrucano and Paleozoic Formations of Southern Tuscany and Northern Latium (Italy). In: Falke, H. (Ed.), The Continental Permian in Central, West, and South Europe. Springer, Netherlands, Dordrecht, pp. 181–195. https://doi.org/10.1007/978-94-010-1461-8_15.

Balestrieri, M.L., Pandeli, E., Bigazzi, G., Carosi, R., Montomoli, C., 2011. Age and temperature constraints on metamorphism and exhumation of the syn-orogenic metamorphic complexes of Northern Apennines, Italy. Tectonophysics 509, 254–271. https://doi.org/10.1016/j.tecto.2011.06.015.

Bertini, G., Cameli, G.M., Costantini, A., Decandia, F.A., Dini, I., Elter, F.M., Lazzarotto, A., Liotta, D., Pandeli, E., Sandrelli, F., 1994. Structural features of southern Tuscany along the Monti di Campiglia-Rapolano Terme cross section. Memorie Della Societa'Geologica Italiana 48, 51–59.

Bianco, C., Godard, G., Halton, A., Brogi, A., Liotta, D., Caggianelli, A., 2019. The lawsonite-glaucophane blueschists of Elba Island (Italy). Lithos 348, 105198.

Bonini, M., Sani, F., Stucchi, E.M., Moratti, G., Benvenuti, M., Menanno, G., Tanini, C., 2014. Late Miocene shortening of the Northern Apennines back-arc. J. Geodyn. 74, 1–31. https://doi.org/10.1016/j.jog.2013.11.002.

Bosio, G., Malinverno, E., Villa, I.M., Di Celma, C., Gariboldi, K., Gioncada, A., Barberini, V., Urbina, M., Bianucci, G., 2020. Tephrochronology and chronostratigraphy of the Miocene Chilcatay and Pisco formations (East Pisco basin, Peru). Newsl. Stratigr. 213–247.

Brogi, A., Giorgetti, G., 2012. Tectono-metamorphic evolution of the siliciclastic units in the Middle Tuscan Range (inner Northern Apennines): Mg–carpholite bearing quartz veins related to syn-metamorphic syn-orogenic foliation. Tectonophysics 526, 167–184.

Brun, J.-P., Faccenna, C., 2008. Exhumation of high-pressure rocks driven by slab rollback. Earth Planet. Sci. Lett. 272, 1–7.

Brunet, C., Monié, P., Jolivet, L., Cadet, J.-P., 2000. Migration of compression and extension in the Tyrrhenian Sea, insights from 40 Ar/39 Ar ages on micas along a transect from Corsica to Tuscany. Tectonophysics 321, 127–155.

Buick, I.S., Holland, T.J.B., 1989. The PTt path associated with crustal extension, Naxos, Cyclades, Greece. Geol. Soc. Lond. Spec. Publ. 43, 365–369.

Capezzuoli, E., Spina, A., Brogi, A., Liotta, D., Bagnoli, G., Zucchi, M., Molli, G., Regoli, R., 2021. Reconsidering the Variscan Basement of Southern Tuscany (Inner Northern Apennines). Geosciences. https://doi.org/10.3390/geosciences11020084.

Carmignani, L., Decandia, F.A., Fantozzi, P.L., Lazzarotto, A., Liotta, D., Meccheri, M., 1994. Tertiary extensional tectonics in Tuscany (northern Apennines, Italy). Tectonophysics 238, 295–315.

Carmignani, L., Kligfield, R., 1990. Crustal extension in the northern Apennines: The transition from compression to extension in the Alpi Apuane Core Complex. Tectonics 9 (6), 1275–1303. https://doi.org/10.1029/TC009i006p01275.

Carminati, E., Doglioni, C., 2012. Alps vs. Apennines: the paradigm of a tectonically asymmetric Earth. Earth Sci. Rev. 112, 67–96. https://doi.org/10.1016/j.earscirev.2012.02.004.

Carosi, R., Montomoli, C., Pertusati, P.C., 2004. Late tectonic evolution of the Northern Apennines: the role of contractional tectonics in the exhumation of the tuscan units. Geodin. Acta 17, 253–273. https://doi.org/10.3166/ga.17.253-273.

Casini, G., Decandia, F.A., Tavarnelli, E., 2007. Analysis of a mesoscopic duplex in SW Tuscany, Italy: implications for thrust system development during positive tectonic inversion. Geol. Soc. Lond. Spec. Publ. 272, 437–446.

Casini, G., Decandia, F.A., Tavarnelli, E., 2008. Pre-orogenic extensional deformations within Permian-Triassic rocks of Southern Tuscany: structural record of an episode of Early Mesozoic continental rifting? Bollettino della Societa Geologica Italiana (Italian Journal of Geosciences) 127, 615–624.

Chafe, A.N., Villa, I.M., Hanchar, J.M., Wirth, R., 2014. A re-examination of petrogenesis and 40 Ar/39 Ar systematics in the Chain of Ponds K-feldspar:"diffusion domain" archetype versus polyphase hygrochronology. Contrib. Mineral. Petrol. 167, 1–17.

Cloos, M., 1982. Flow melanges: numerical modeling and geologic constraints on their origin in the Franciscan subduction complex, California. GSA Bull. 93, 330–345. https://doi.org/10.1130/0016-7606(1982)93<330:FMNMAG>2.0.CO;2.

Conti, P., Costantini, A., Tongiorgi, M., Di Pisa, A., Decandia, F.A., 1991. Structural frame of the Tuscan Paleozoic: a review. Boll. Soc. Geol. Ital. 110, 523–541.

Conti, P., Cornamusini, G., Carmignani, L., 2020. An outline of the geology of the Northern Apennines (Italy), with geological map at 1: 250,000 scale. Ital. J. Geosci. 139, 149–194.

Costantini, A., Decandia, F.A., Lazzarotto, A., Sandrelli, F., 1988. L'unità di Monticiano-Roccastrada fra la Montagnola senese ed il Monte Leoni (Toscana meridionale). Atti Ticinensi di Scienze della Terra 31, 382–420.

Davis, D., Suppe, J., Dahlen, F.A., 1983. Mechanics of fold-and-thrust belts and accretionary wedges. J. Geophys. Res. Solid Earth 88, 1153–1172. https://doi.org/10.1029/JB088iB02p01153.

Deino, A., Keller, J.V.A., Minelli, G., Pialli, G., 1992. Datazioni 40Ar/39Ar del metamorfismo dell'Unità di Ortano-Rio Marina (Isola d'Elba): risultati preliminari. Studi Geol. Camerti 2, 187–192.

Dewey, J.F., 1980. Episodicity, sequence and style at convergent plate boundaries. The continental crust and its mineral deposits.

Di Vincenzo, G., Godard, G., Molli, G., 2022. Dating low-grade deformation: role of lithology and strain partitioning on Ar isotope records in the Alpi Apuane of Northern Apennines (Italy). Tectonics 41, e2022TC007248. https://doi.org/10.1029/2022TC007248.

Engi, M., Lanari, P., Kohn, M.J., 2017. Significant Ages—an Introduction to Petrochronology. Rev. Mineral. Geochem. 83, 1–12. https://doi.org/10.2138/rmg.2017.83.1.

England, P.C., Holland, T.J.B., 1979. Archimedes and the Tauern eclogites: the role of buoyancy in the preservation of exotic eclogite blocks. Earth Planet. Sci. Lett. 44, 287–294. https://doi.org/10.1016/0012-821X(79)90177-8.

Fellin, M.G., Reiners, P.W., Brandon, M.T., Wu, E., Balestrieri, M.L., Molli, G., 2007. Thermochronologic evidence for the exhumational history of the Alpi Apuane metamorphic core complex, northern Apennines. Italy 26. https://doi.org/10.1029/2006TC002085.

Foland, K.A., 1983. 40Ar/39Ar incremental heating plateaus for biotites with excess argon. Chem. Geol. 41, 3–21.

Giglia, G., Radicati di Brozolo, F., 1970. K/Ar age of metamorphism in the Apuane Alps (Northern Tuscany). Boll. Soc. Geol. Ital. 89, 485–497.

Giorgetti, G., Goffe, B., Memmi, I., Nieto, F., 1998. Metamorphic evolution of Verrucano metasediments in Northern Apennines; new petrological constraints. Eur. J. Mineral. 10, 1295–1308.

Giuntoli, F., Viola, G., 2021. Cyclic brittle-ductile oscillations recorded in exhumed high-pressure continental units: a record of deep episodic tremor and slow slip events in the Northern Apennines. Geochem. Geophys. Geosyst. 22.

Giuntoli, F., Viola, G., 2022. A likely geological record of deep tremor and slow slip events from a subducted continental broken formation. Sci. Rep. 12 https://doi.org/10.1038/s41598-022-08489-2.

Giuntoli, F., Menegon, L., Warren, C.J., Darling, J., Anderson, M.W., 2020. Protracted shearing at midcrustal conditions during large-scale thrusting in the scandinavian caledonides. Tectonics 39, e2020TC006267. https://doi.org/10.1029/2020TC006267.

Giuntoli, F., Viola, G., Sørensen, B.E., 2022. Deformation mechanisms of blueschist facies continental metasediments may offer insights into deep episodic tremor and slow slip events. J. Geophys. Res. Solid Earth 127. https://doi.org/10.1029/2022JB024265.

Hodges, K.V., Harries, W.E., Bowring, S.A., 1994. 40Ar/39Ar age gradients in micas from a high-temperature-low-pressure metamorphic terrain: evidence for very slow cooling and implications for the interpretation of age spectra. Geology 22, 55–58. https://doi.org/10.1130/0091-7613(1994)022<0055:AAAGIM>2.3.CO;2.

Jacobs, J., Paoli, G., Rocchi, S., Ksienzyk, A.K., Sirevaag, H., Elburg, M.A., 2018. Alps to Apennines zircon roller coaster along the Adria microplate margin. Sci. Rep. 8, 2704. https://doi.org/10.1038/s41598-018-20979-w.

Jolivet, L., Faccenna, C., Goffé, B., Mattei, M., Rossetti, F., Brunet, C., Storti, F., Funiciello, R., Cadet, J.P., D'Agostino, N., 1998. Midcrustal shear zones in postorogenic extension: example from the northern Tyrrhenian Sea. J. Geophys. Res. Solid Earth 103, 12123–12160.

Keller, J.V.A., Pialli, G., 1990. Tectonics of the Island of Elba: a reappraisal. Boll. Soc. Geol. Ital. 109, 413–425.

Kligfield, R., Hunziker, J., Dallmeyer, R.D., Schamel, S., 1986. Dating of deformation phases using K-Ar and 40Ar/39Ar techniques: results from the Northern Apennines. J. Struct. Geol. 8, 781–798.

Kurz, W., Froitzheim, N., 2002. The exhumation of eclogite-facies metamorphic rocks—a review of models confronted with examples from the alps. Int. Geol. Rev. 44, 702–743. https://doi.org/10.2747/0020-6814.44.8.702.

Lanari, P., Vidal, O., Lewin, E., Dubacq, B., De Andrade, V., Schwartz, S., 2014. XMapTools a Matlab©-based graphic user interface for microprobe quantified image processing. Comput. Geosci. 62, 227–240. https://doi.org/10.1016/j.cageo.2013.08.010.

Lazzarotto, A., Mazzanti, R., Mazzoncini, F., 1964. Geologia del promontorio Argentario (Grosseto) e del promontorio del Franco (Isola del Giglio-Grosseto). Boll. Soc. Geol. Ital. 83, l–l24.

Lazzarotto, A., Aldinucci, M., Cirilli, S., Costantini, A., Decandia, F.A., Pandeli, E., Sandrelli, F., Spina, A., 2003. Stratigraphic correlation of the Upper Palaeozoic-Triassic successions in southern Tuscany, Italy. Bollettino della Società Geologica Italiana, Special Volumes 2, 25–35.

Lister, G.S., Davis, G.A., 1989. The origin of metamorphic core complexes and detachment faults formed during Tertiary continental extension in the northern Colorado River region, U.S.A. J. Struct. Geol. 11, 65–94. https://doi.org/10.1016/0191-8141(89)90036-9.

Malusà, M.G., Fitzgerald, P.G., 2019. Fission-Track Thermochronology and its Application to Geology. Springer.

Maruyama, S., Liou, J.G., Terabayashi, M., 1996. Blueschists and eclogites of the world and their exhumation. Int. Geol. Rev. 38, 485–594. https://doi.org/10.1080/00206819709465347.

Massa, G., Musumeci, G., Mazzarini, F., Pieruccioni, D., Centro, C.G.T., Valdarno, S.G., 2017. Coexistence of contractional and extensional tectonics during the northern Apennines orogeny: the late Miocene out-of-sequence thrust in the Elba Island nappe stack. Geol. J. 52, 353–368. https://doi.org/10.1002/gj.

Molli, G., 2008. Northern Apennine–Corsica orogenic system: an updated overview. Geol. Soc. Lond. Spec. Publ. 298, 413–442.

Molli, G., Giorgetti, G., Meccheri, M., 2000. Structural and petrological constraints on the tectono-metamorphic evolution of the Massa Unit (Alpi Apuane, NW Tuscany, Italy). Geol. J. 35, 251–264.

Molli, G., Carlini, M., Vescovi, P., Artoni, A., Balsamo, F., Camurri, F., Clemenzi, L., Storti, F., Torelli, L., 2018a. Neogene 3-D structural architecture of the north-west apennines: the role of the low-angle normal faults and basement thrusts. Tectonics 37, 2165–2196.

Molli, G., Vitale Brovarone, A., Beyssac, O., Cinquini, I., 2018b. RSCM thermometry in the Alpi Apuane (NW Tuscany, Italy): new constraints for the metamorphic and tectonic history of the inner northern Apennines. J. Struct. Geol. 113, 200–216. https://doi.org/10.1016/j.jsg.2018.05.020.

Montemagni, C., Montomoli, C., Iaccarino, S., Carosi, R., Jain, A.K., Massonne, H.-J., Villa, I.M., 2019. Dating protracted fault activities: microstructures, microchemistry and geochronology of the Vaikrita Thrust, Main Central Thrust zone, Garhwal Himalaya, NW India. Geol. Soc. Lond. Spec. Publ. 481, 127–146. https://doi.org/10.1144/SP481.3.

Montomoli, C., Carosi, R., Pertusati, P.C., 2009. Tectonic history of the Monti dell'Uccellina range, Southern Tuscany, Italy. Boll. Soc. Geol. Ital. 128, 515–526.

Morley, C.K., 1988. Out-of-sequence thrusts. Tectonics 7, 539–561.

Mulch, A., Cosca, M., Andresen, A., Fiebig, J., 2005. Time scales of deformation and exhumation in extensional detachment systems determined by high-spatial resolution in situ UV-laser 40Ar/39Ar dating. Earth Planet. Sci. Lett. 233, 375–390. https://doi.org/10.1016/j.epsl.2005.01.042.

Musumeci, G., Mazzarini, F., Cruden, A.R., 2015. The Zuccale Fault, Elba Island, Italy: a new perspective from fault architecture. Tectonics 34, 1195–1218. https://doi.org/10.1002/2014TC003809.

Papeschi, S., Musumeci, G., Massonne, H.-J., Mazzarini, F., Ryan, E.J., Viola, G., 2020. High-P (P = 1.5–1.8 GPa) blueschist from Elba: implications for underthrusting and exhumation of continental units in the Northern Apennines. J. Metamorph. Geol. 38, 495–525. https://doi.org/10.1111/jmg.12530.

Platt, J.P., 1986. Dynamics of orogenic wedges and the uplift of high-pressure metamorphic rocks. GSA Bull. 97, 1037–1053. https://doi.org/10.1130/0016-7606(1986)97<1037:DOOWAT>2.0.CO;2.

Platt, J., 1993. Exhumation of high-pressure rocks: a review of concepts and processes. Terra Nova 5, 119–133.

Radicati di Brozolo, F., Giglia, G., 1973. Further data on the Corsica–Sardinia rotation. Nature 241, 389–391.

Rama, S.N.I., Hart, S.R., Roedder, E., 1965. Excess radiogenic argon in fluid inclusions. J. Geophys. Res. 70, 509–511.

Rivera, T.A., Storey, M., Zeeden, C., Hilgen, F.J., Kuiper, K., 2011. A refined astronomically calibrated 40Ar/39Ar age for Fish Canyon sanidine. Earth Planet. Sci. Lett. 311, 420–426.

Rolland, Y., Cox, S.F., Corsini, M., 2009. Constraining deformation stages in brittle – ductile shear zones from combined field mapping and 40 Ar / 39 Ar dating : the structural evolution of the Grimsel Pass area (Aar Massif, Swiss Alps). J. Struct. Geol. 31, 1377–1394. https://doi.org/10.1016/j.jsg.2009.08.003.

Rossetti, F., Faccenna, C., Jolivet, L., Funiciello, R., Tecce, F., Brunet, C., 1999. Syn-versus post-orogenic extension: the case study of Giglio Island (Northern Tyrrhenian Sea, Italy). Tectonophysics 304, 71–93.

Rossetti, F., Faccenna, C., Jolivet, L., Funiciello, R., Goffé, B., Tecce, F., Brunet, C., Monié, P., Vidal, O., 2001. Structural signature and exhumation PTt path of the Gorgona blueschist sequence (Tuscan archipelago, Italy). Ofioliti 26, 175–186.

Rossetti, F., Faccenna, C., Jolivet, L., Goffé, B., Funiciello, R., 2002. Structural signature and exhumation PTt paths of the blueschist units exposed in the interior of the Northern Apennine chain, tectonic implications. Boll. Soc. Geol. Ital. 121, 829–842.

Ryan, E., Papeschi, S., Viola, G., Musumeci, G., Mazzarini, F., Torgersen, E., Sørensen, B. E., Ganerød, M., 2021. Syn-orogenic exhumation of high-P units by upward extrusion in an accretionary wedge: insights from the Eastern Elba Nappe Stack (Northern Apennines, Italy). Tectonics 40, e2020TC006348. https://doi.org/10.1029/2020TC006348.

Steiger, R.H., Jäger, E., 1977. Subcommission on geochronology: convention on the use of decay constants in geo-and cosmochronology. Earth Planet. Sci. Lett. 36, 359–362.

Storti, F., 1995. Tectonics of the Punta Bianca promontory: insights for the evolution of the Northern Apennines-Northern Tyrrhenian Sea basin. Tectonics 14, 832–847.

Tagami, T., Galbraith, R.F., Yamada, R., Laslett, G.M., 1998. Revised annealing kinetics of fission tracks in zircon and geological implications. In: Advances in Fission-Track Geochronology: A Selection of Papers Presented at the International Workshop on Fission-Track Dating, Ghent, Belgium, 1996. Springer, pp. 99–112.

Theye, T., Reinhardt, J., Goffé, B., Jolivet, L., Brunet, C., 1997. Ferro- and magnesiocarpholite from the Monte Argentario (Italy): first evidence for high-pressure metamorphism of the metasedimentary Verrucano sequence, and significance for P-T path reconstruction. Eur. J. Mineral. 9, 859–874. https://doi.org/10.1127/ejm/9/4/0859.

Villa, I.M., Bosio, G., 2022. "Excess Ar" by laboratory alteration of biotite. Geology 51, 121–125. https://doi.org/10.1130/G50503.1.

Villa, I.M., Hanchar, J.M., 2017. Age discordance and mineralogy. Am. Mineral. 102, 2422–2439. https://doi.org/10.2138/am-2017-6084.

Villa, I.M., Hermann, J., Muentener, O., Trommsdorff, V., 2000. 39Ar-40 Ar dating of multiply zoned amphibole generations (Malenco, Italian Alps). Contrib. Mineral. Petrol. 140, 363–381.

Villa, I.M., Bucher, S., Bousquet, R., Kleinhanns, I.C., Schmid, S.M., 2014. Dating polygenetic metamorphic assemblages along a transect across the Western Alps. J. Petrol. 55, 803–830. https://doi.org/10.1093/petrology/egu007.

Villa, I.M., Glodny, J., Peillod, A., Skelton, A., Ring, U., 2023. Petrochronology of polygenetic white micas (Naxos, Greece). J. Metamorph. Geol. 41, 401–423. https://doi.org/10.1111/jmg.12700.

Viola, G., Henderson, I.H.C., Bingen, B., Hendriks, B.W.H., 2011. The Grenvillian – Sveconorwegian orogeny in Fennoscandia : back-thrusting and extensional shearing along the " Mylonite Zone ", 189, 368–388. https://doi.org/10.1016/j.precamres.2011.06.005.

Viola, G., Torgersen, E., Mazzarini, F., Musumeci, G., van der Lelij, R., Schönenberger, J., Garofalo, P.S., 2018. New constraints on the evolution of the inner Northern Apennines by K-Ar dating of Late Miocene-Early Pliocene compression on the Island of Elba, Italy. Tectonics 37, 3229–3243.

Viola, G., Musumeci, G., Mazzarini, F., Tavazzani, L., Curzi, M., Torgersen, E., van der Lelij, R., Aldega, L., 2022. Structural characterization and K–Ar illite dating of reactivated, complex and heterogeneous fault zones: lessons from the Zuccale Fault, Northern Apennines. Solid Earth 13, 1327–1351. https://doi.org/10.5194/se-13-1327-2022.

Walters, J.B., Kohn, M.J., 2017. Protracted thrusting followed by late rapid cooling of the Greater Himalayan Sequence, Annapurna Himalaya, Central Nepal: insights from titanite petrochronology. J. Metamorph. Geol. 35, 897–917.

Warren, C.J., Hanke, F., Kelley, S.P., 2012a. When can muscovite 40 Ar/39 Ar dating constrain the timing of metamorphic exhumation? Chem. Geol. 291, 79–86.

Warren, C.J., Smye, A.J., Kelley, S.P., Sherlock, S.C., 2012b. Using white mica 40Ar/39Ar data as a tracer for fluid flow and permeability under high-P conditions: Tauern Window, Eastern Alps. J. Metamorph. Geol. 30, 63–80. https://doi.org/10.1111/j.1525-1314.2011.00956.x.

Westerman, D.S., Innocenti, F., Tonarini, S., Ferrara, G., 1993. The Pliocene intrusions of the Island of Giglio. Mem. Soc. Geol. Ital. 49, 345–363.